ELSEVIER

Chemical Geology 208 (2004) 29–59

CHEMICAL GEOLOGY
INCLUDING
ISOTOPE GEOSCIENCE

www.elsevier.com/locate/chemgeo

Re–Os isotope systematics and platinum group element fractionation during mantle melt extraction: a study of massif and xenolith peridotite suites

D.G. Pearson[a,*], G.J. Irvine[a], D.A. Ionov[b], F.R. Boyd[c], G.E. Dreibus[d]

[a] *Arthur Holmes Isotope Geology Laboratory, Department of Geological Sciences, Durham University, South Road, Durham, DH1 3LE, UK*
[b] *Laboratoire de Tectonophysique, ISTEEM, CC 49, Université de Montpellier 2, pl. E. Bataillon, 34095 Montpellier Cedex 05, France*
[c] *Geophysical Laboratory, Carnegie Institution of Washington, 5251 Broad Branch Road, NW, Washington, DC 20015, USA*
[d] *Cosmochemistry, Max Plank Institute fur Chemie, Saarstrasse 23, Mainz, 6500, Germany*

Abstract

Re–Os isotope and platinum group elements (PGE) systematics are presented for peridotite xenoliths from N. Lesotho (on-craton), S. Namibia (circum-cratonic), the Vitim volcanic field (Baikhal Rift), plus massif peridotites from Beni Bousera, N. Morocco. Mg–Fe variations indicate that these samples have experienced between 5% (Vitim–Beni Bousera) and 50% (Lesotho) melt extraction, providing the opportunity to examine PGE fractionation over a large melting interval. The Namibian xenoliths and Beni Bousera massif peridotites show no variation of iridium group (Ir, Ru, Os; I-PGE) abundances or inter-element fractionations relative to melt depletion indices such as Mg number or Al_2O_3. Lesotho peridotites show large variations in I-PGE abundances (Os range 0.2–13 ppb) at relatively constant Al_2O_3 that are not easily rationalised by melt-extraction models. Despite these abundance variations, there is no significant inter-element fractionation of I-PGE, e.g., $(Os/Ir)_n$, showing that these elements are not fractionated by even very large degrees of melting (up to 50% melt extraction). Lesotho peridotites are amongst the most P-PGE (Pt, Pd)-depleted mantle rocks, with highly fractionated chondrite-normalised PGE. PGE systematics for all these peridotite suites allow a relative order of PGE compatibility to be firmly established for mantle melting:

$$D^{Os}_{solid/melt} \sim D^{Ir}_{solid/melt} \sim D^{Ru}_{solid/melt} > D^{Pt}_{solid/melt} > D^{Pd}_{solid/melt}.$$

Vitim peridotite xenoliths have very low Os contents and low Os/Ir (< 70% chondritic) compared to the kimberlite-borne xenoliths and massif peridotites. The Vitim low Os/Ir is comparable with other suites of alkali-basalt-borne peridotite xenoliths and may result from syn- or post-eruption sulphide breakdown and alteration. Chondritic $(Ru/Ir)_n$ and $(Os/Ir)_n$ ratios in Lesotho and other cratonic peridotites show no evidence of anomalous PGE fractionations in the Archean subcontinental mantle and support the Late Veneer hypothesis. In most of the peridotite suites, $(Pd/Ir)_n$ values show a strong correlation with Os isotopic composition that is likely the result of melt-residue interaction. The positive variation of both $(Ru/Ir)_n$ and $(Pd/Ir)_n$ with bulk rock Al_2O_3 and Os isotopic composition for Beni Bousera and global massif peridotites indicates that these PGE ratios were modified by interaction with melts. Hence, we find no support for the intra-element PGE fractionation in the continental lithospheric mantle (CLM) representing primordial mantle heterogeneity. Highly

* Corresponding author.

0009-2541/$ - see front matter
doi:10.1016/j.chemgeo.2004.04.005

unradiogenic Os isotope compositions appear characteristic of lithospheric peridotites with the lowest $(Pd/Ir)_n$. In these samples, bulk-rock PGE patterns suggest that Os isotope systematics should be dominated by primary, residual, P-PGE-depleted sulphides, and hence, their bulk rock Re-depletion ages should be expected to approximate the melting age of the rock.

Keywords: Re–Os isotope; Platinum group element; Mantle melt extraction

1. Introduction

The relative fractionation of platinum group elements (PGE) in mantle samples has received an increasing amount of attention recently because of their potential to constrain the processes that affected the generation and evolution of the mantle (e.g., Morgan et al., 1981; Pattou et al., 1996; Snow and Schmidt, 1998). Much debate has centred on the significance and implications of inter-element PGE fractionations that appear to be common in parts of the continental lithospheric mantle (CLM) as sampled by orogenic lherzolites in particular. Two end-member views have developed. One perspective is that the non-chondritic inter-element PGE fractionations are an inherent feature of certain parts of the mantle (e.g., Pattou et al., 1996; Snow and Schmidt, 1998; Lorand et al., 1999, 2000). This interpretation carries with it important implications for the Late Veneer model of mantle evolution. The alternate view is that these fractionations are due to recent melt infiltration processes in the lithosphere and hence have no bearing on the heterogeneity and processes occurring in the deep mantle (Brandon et al., 1998; Rehkämper et al., 1999a).

To date, most data relating to this argument have been obtained on orogenic lherzolite massifs and abyssal peridotites (e.g., Pattou et al., 1996; Lorand et al., 1999, 2000; Rehkämper et al., 1999a) with some data from spinel-facies peridotites erupted in continental rifts (e.g., Rehkämper et al., 1997, Handler and Bennett, 1999; Lorand and Alard, 2001; Lee, 2002). Initial indications are that off-craton spinel lherzolites do not possess the inter-element PGE fractionations shown by orogenic lherzolites (Handler and Bennett, 1999; Lorand and Alard, 2001). This data set requires broader comparison with samples of older, cratonic lithosphere, for which very little PGE data exists. Cratonic peridotites record melting events that are significantly older than orogenic lherzolites and most spinel-facies peridotites from continental rifts (e.g., Pearson, 1999a,b) and so offer the possibility to examine how widespread PGE fractionations are in the CLM and whether these elemental variations can be traced back into the Archean. Furthermore, cratonic peridotites represent the residues from much larger degrees of melting than most other peridotites (e.g., Boyd, 1989; Walter, 2003) and so provide the opportunity to examine inter-element PGE fractionation at very large degrees of melting.

To examine these issues further, Re–Os isotopes and PGE concentrations have been determined for a suite of 35 cratonic peridotite xenoliths from the kimberlites of N. Lesotho, 6 circum-cratonic kimberlite-borne peridotite xenoliths from Namibia (15 analysed for Re–Os), 12 peridotite xenoliths from the Vitim volcanic field, Baikal rift zone, Siberia, and 6 orogenic peridotites from the Beni Bousera peridotite massif, N. Morocco. The data allow examination of the interrelationship between PGE and Re–Os fractionations during mantle processes. The various sample suites were isolated into the CLM over a range of time, from the Archean (N. Lesotho), to the mid-Proterozoic (Beni Bousera) and so allow tracing of mantle PGE systematics over a period of >1.5 Gyr.

2. Samples and petrological background

All samples selected for this study had been previously characterised for petrography, major and trace-element chemistry. For completeness and accessibility of data, the previously published major-element chemistry for some samples (Namibia and Vitim) are presented alongside new, unpublished data

in Table 1. Aspects of the major-element and PGE chemistry are summarized in Table 2. Calculated modal analyses for all rocks analysed are available on request from the authors.

2.1. Constraining the extent of partial melting and melt re-addition

The major-element composition of peridotites allows estimation of the degree of melt extraction they have experienced. We use an approach based on constraints from experimental petrology and major-element parameters, outlined by Walter (1999, 2003). This method uses bulk rock MgO–FeO characteristics and gives qualitatively similar results to those employed by Frey et al. (1985) but has the advantage of being able to place some constraints on the likely pressure of melting (Fig. 1). Many cratonic and circum-cratonic, kimberlite-borne xenoliths contain small amounts of introduced Fe, distributed along grain boundaries (e.g., Boyd et al., 1997). This can vary between 0% and 0.5% FeO for low-temperature peridotites. The overall effect is to decrease the estimated degree and pressure of melting. The process could produce some of spread in the Lesotho data (Fig. 1), and so, the extents and pressures of melting could be minima. Alternative approaches use Ca and Al to estimate extents of melt extraction (Walter, 1999, 2003). The likely introduction of diopside to the Lesotho and Namibia garnet peridotites (e.g., Simon et al., 2003; Boyd et al., 2004) will have dramatic consequences for bulk rock Ca and Al values, but will leave MgO–FeO systematics largely unaffected because of the high Mg number of mantle diopsides. Furthermore, the Vitim suite contains samples with markedly sub- and supra-chondritic Ca/Al (0.47–1.42). Sub-chondritic Ca/Al can be a likely consequence of the extraction of diopside (Ca/Al: 4 to >10) during partial melting. Supra-chondritic Ca/Al is a characteristic of off-craton peridotite xenoliths worldwide (Pearson et al., 2003), and this feature can be interpreted as a result of the crystallisation of diopside during melt percolation through lithosphere. This is supported by the LREE enriched nature of many of the diopsides. For these reasons, we use Mg–Fe systematics as the most reliable indicator of the degree of melt depletion.

2.2. N. Lesotho peridotite xenoliths

The N. Lesotho suite has been the subject of a detailed Re–Os isotopic (Irvine et al., 2001; Irvine, 2002) and mineral trace-element studies (Simon et al., 2003). Most samples are granular, low-temperature garnet lherzolites and harzburgites. Several spinel-facies peridotites were analysed. The majority of xenoliths are from the Letseng kimberlite. Smaller subsuites are from the Matsoku, Liqhobong and Thaba Putsoa kimberlites. All these kimberlites erupted on the SE margin of the Kaapvaal craton ~ 90 Myr ago (Davis et al., 1976).

The N. Lesotho peridotite suite is typical of cratonic peridotites from southern Africa. Most samples have highly depleted major-element compositions, i.e., they are depleted in "basaltic" components such as FeO (Fig. 1). This is manifest by very high average Mg numbers of olivine (92.7 ± 1; Table 2; typical cratonic peridotite worldwide = 92.6; e.g., Pearson et al., 2003) and very low average Al_2O_3 contents (1.14 wt.%; Table 2). This depleted major-element character is indicative of very large degrees (>30–50%) of melt extraction at high pressures (>5 GPa; e.g., Boyd, 1989; Walter, 1999, 2003; Fig. 1). Incompatible trace elements show that cratonic peridotite xenoliths have experienced multistage histories involving later metasomatic additions, superimposed on the initial melt depletion.

2.3. Namibian peridotite xenoliths

This suite is exclusively from the Farm Louwrencia kimberlite, erupted through basement of meso-Proterozoic age in S. central Namibia (Hoal et al., 1995). Petrography and major-element data for this xenolith suite have been presented by Boyd et al. (2004). Samples show a range in equilibration temperatures of 800–1300 °C. Equilibration pressures suggest depths of derivation ranging from ~ 75 to 150 km and define a roughly cratonic (40 mW m^{-2}) geotherm (Boyd et al., 2004).

All but one specimen are of the granular, low-*T* category, dominantly garnet lherzolites. Bulk compositions are slightly less depleted than the N. Lesotho suite, reflected in slightly lower average olivine Mg number (91.7 ± 0.4; Table 2) and slightly higher Al_2O_3 contents (1.21 wt.%; Table 2). Hence, the

Table 1
Major element, Re–Os isotope and PGE data

Beni Bousera									
Sample	GP13	GP91	GP132(3)	GP189	GP191	GP220	GP178	GP222	GP240
Lithology	S-L	S-L/H	S-L	S-L	S-L	S-L	S-L/H	S-L	S-L
SiO_2 (wt.%)	44.91	43.91	42.99	44.29	44.13	43.91	42.78	44.89	44.73
TiO_2 (wt.%)	0.14	0.02	0.03	0.04	0.11	0.02	0.05	0.12	0.11
Al_2O_3 (wt.%)	3.45	0.72	1.28	2.04	3.09	1.61	0.91	2.89	3.13
FeO (wt.%)	8.19	8.27	8.13	7.86	8.29	7.6	8.13	8.05	8.01
MnO (wt.%)	0.15	0.14	0.14	0.14	0.15	0.14	0.13	0.15	0.14
MgO (wt.%)	39.79	46.35	46.11	43.63	41.11	44.68	46.99	41.17	40.73
CaO (wt.%)	3.01	0.56	0.82	1.88	2.8	1.44	0.83	2.43	2.61
Na_2O (wt.%)	0.3	0	0.47	0.1	0.31	0.58	0.15	0.31	0.51
Re (ppb)	0.330	0.089	0.076	0.168	0.268	0.028	0.191	0.201	0.252
Os (ppb)	3.578	17.522	4.53	3.44	3.63	0.9195	3.28	3.41	3.79
$^{187}Re/^{188}Os$	0.4441	0.0244	0.08029	0.2354	0.3553	0.1444	0.284	0.284	0.320
$^{187}Os/^{188}Os$	0.1262	0.1209	0.1204	0.1209	0.1243	0.1214	0.1226	0.1240	0.1240
Pd (ppb)	5.85	6.58	2.07	5.40	6.48	4.46			
Pt (ppb)	6.65	7.03	9.72	6.77	6.70	4.39			
Ru (ppb)	6.71	7.4	7.46	6.49	6.36	0.403			
Ir (ppb)	3.28	4.70	4.15	3.23	3.27	3.36			

Lesotho	Letseng											
Sample	LET2	LET6	LET8	LET12	LET13	LET14	LET25	LET27	LET28	LET29	LET30	LET31
Lithology	G-H	S-H	S-H	G-H	G-S-L	G-S-H	S-L	G-L	S-H	G-H	G-H	G-L
SiO_2 (wt.%)	45.45	45.55	46.20	47.22	46.28	47.46	45.20	46.79	46.02	46.32	46.18	47.26
TiO_2 (wt.%)	0.04	0.15	0.01	0.02	0.07	0.04	0.04	0.11	0.01	0.02	0.04	0.05
Al_2O_3 (wt.%)	0.60	0.88	0.58	0.89	0.96	0.77	0.70	1.37	0.60	1.05	1.32	1.08
FeO (wt.%)	6.22	6.62	5.89	6.70	6.40	5.93	6.90	6.55	6.46	6.45	6.53	6.64
MnO (wt.%)	0.10	0.13	0.10	0.12	0.13	0.11	0.12	0.13	0.12	0.11	0.13	0.13
MgO (wt.%)	46.82	45.15	46.86	43.82	45.37	44.95	46.28	43.69	46.15	44.92	44.64	43.72
CaO (wt.%)	0.38	0.71	0.18	0.91	0.48	0.37	0.41	0.82	0.27	0.78	0.78	0.79
Na_2O (wt.%)	0.07	0.13	0.04	0.05	0.05	0.06	0.05	0.11	0.05	0.08	0.08	0.11
Re (ppb)	0.330	0.137	0.251	0.153	0.041	0.089	0.150	0.367	0.096	0.260	0.217	0.201
Os (ppb)	5.71	3.18	1.60	3.16	3.31	4.70	1.98	6.25	3.88	3.44	2.37	5.82
$^{187}Re/^{188}Os$		0.207	0.753	0.232	0.059	0.091	0.415	0.282	0.119	0.362	0.438	0.166
$^{187}Os/^{188}Os$		0.1088	0.1086	0.1095	0.1086	0.1086	0.1083	0.1090	0.1079	0.1101	0.1130	0.1097
Pd (ppb)	0.732	0.035	0.093	0.074	0.022	0.378	0.121	0.102	0.028	0.211	0.111	0.518
Pt (ppb)	3.76	0.182	0.288	0.535	0.886	1.50	2.12	3.92	2.40	1.41	0.225	2.69
Ru (ppb)	8.17	1.42	2.16	4.44	4.70	6.19	3.65	8.12	5.41	2.45	2.38	7.74
Ir (ppb)	5.26	1.72	1.89	2.65	3.37	4.69	2.22	5.44	3.33	1.71	2.33	4.12
S (ppm)	203	345	161	188	158	130	351	274	381	128	145	266

Lesotho								Thaba Putsoa				
Sample	LET38	LET47	LET48	LET49	LET58	LET63	LET64	TP5	TP6	TP7	TP9	LQ1
Lithology	G-L	G-S-L	G-L	G-L	G-L	G-L	G-L	G-L	G-S-L	G-S-H	G-S-L	G-L
SiO_2 (wt.%)	48.18	46.64	46.90	44.19	45.63	42.89	47.96	46.31	45.82	45.85	46.36	45.18
TiO_2 (wt.%)	0.02	0.01	0.03	0.07	0.09	0.03	0.08	0.02	0.01	0.21	0.01	0.04
Al_2O_3 (wt.%)	1.57	0.88	0.90	1.57	1.05	0.61	1.80	1.23	0.67	1.06	0.89	1.17
FeO (wt.%)	5.96	6.79	6.61	8.16	7.41	8.71	6.17	6.25	6.73	7.79	6.63	6.68
MnO (wt.%)	0.12	0.13	0.13	0.15	0.14	0.14	0.13	0.12	0.12	0.12	0.12	0.11
MgO (wt.%)	43.13	44.72	44.13	44.17	44.19	46.72	42.56	45.16	45.99	43.85	45.25	45.94
CaO (wt.%)	0.81	0.50	0.79	1.21	1.05	0.43	0.90	0.72	0.45	0.88	0.55	0.51
Na_2O (wt.%)	0.08	0.06	0.09	0.11	0.09	0.04	0.10	0.08	0.07	0.10	0.07	0.09
Re (ppb)	0.09	0.19	0.23	0.11	0.33	0.09	0.60	0.20	0.02	0.03	0.02	0.01
Os (ppb)	13.7	4.35	1.99	3.86	5.22	4.13	6.42	0.17	5.46	2.44	4.57	0.20
$^{187}Re/^{188}Os$	0.031	0.212	0.545	0.14	0.306	0.104	0.448		0.018	0.064	0.025	0.304
$^{187}Os/^{188}Os$	0.1090	0.1095	0.1162	0.1191	0.1079	0.1191	0.1100		0.1073	0.1082	0.1077	0.1125
Pd (ppb)	0.039	0.028	1.76	5.92	0.851	1.758	0.241	0.024	0.063	0.207	0.104	0.033
Pt (ppb)	9.63	3.32	3.16	6.75	4.29	3.70	7.48	0.201	4.00	0.8	4.29	0.167
Ru (ppb)	15.52	6.39	9.73	7.44	5.71	6.88	10.0	2.54	9.98	2.95	7.25	4.64
Ir (ppb)	8.54	4.27	2.27	3.81	4.17	3.68	6.41	0.303	5.95	2.63	4.51	0.33
S (ppm)	84	127	86	197	92	333	121		90	73	57	295

Lesotho	Liqhobong				Matsoku							
Sample	LQ5	LQ6	LQ8	LQ9	M1	M3	M5	M6	M8	M9	M11	M13
Lithology	G-L	G-L	G-L	G-H	G-S-H	G-L	S-L	S-L	G-S-L	G-L	G-L	G-S-L
SiO_2 (wt.%)	48.14	47.38	47.63	47.95	44.98	44.57	46.45	46.05	46.67	48.01	47.16	46.18
TiO_2 (wt.%)	0.01	0.03	0.01	0.03	0.58	2.50	0.03	0.04	0.04	0.11	0.06	0.07
Al_2O_3 (wt.%)	1.76	1.48	1.22	1.47	0.82	1.98	1.49	1.46	1.46	1.46	1.33	0.86
FeO (wt.%)	4.33	6.36	6.02	6.03	9.93	10.59	6.82	6.85	6.81	6.42	6.36	6.74
MnO (wt.%)	0.12	0.12	0.11	0.11	0.14	0.15	0.12	0.12	0.13	0.13	0.12	0.12
MgO (wt.%)	42.66	43.37	43.99	43.26	42.55	38.93	43.86	44.26	43.79	42.65	43.77	45.06
CaO (wt.%)	0.91	0.94	0.72	0.76	0.58	0.96	0.88	0.91	0.81	0.93	0.84	0.63
Na_2O (wt.%)	0.09	0.13	0.11	0.11	0.12	0.12	0.10	0.10	0.09	0.14	0.12	0.11
Re (ppb)	0.01	0.11	0.01	0.02	0.16	0.26	0.09	0.08	0.08	0.02	0.03	0.03
Os (ppb)	6.57	2.17	3.82	6.68	2.21	0.83	3.16	2.95	4.38	9.55	4.24	5.36
$^{187}Re/^{188}Os$	0.009	0.233		0.012	0.357	1.516	0.137	0.128	0.085	0.007	0.038	0.028
$^{187}Os/^{188}Os$	0.1091	0.1095		0.1080	0.1220	0.1252	0.1118	0.1110	0.1130	0.1085	0.1098	0.1095
Pd (ppb)	0.087	0.304	0.168	0.071	2.69	1.36	1.31	1.02	2.10	0.063	0.331	0.093
Pt (ppb)	2.28	2.42	2.47	4.30	3.37	1.50	3.41	2.79	5.50	6.50	2.26	1.90
Ru (ppb)	8.78	3.93	5.36	12.42	4.23	1.57	5.47	5.21	7.23	9.56	6.03	4.56
Ir (ppb)	6.34	2.98	3.75	7.83	2.27	0.94	3.36	3.29	5.04	7.89	2.35	4.28
S (ppm)	28	60	19	60	122	275	60	43	97	22	56	83

(continued on next page)

Table 1 (*continued*)

Vitim												
Sample	314-72	314-74	314-6	314-58	314-59	313-6	313-54	313-102	313-104	314-5a	314-5b	313-05
Lithology	S-L	G-S-L	S-L	S-L	S-L	G-L	G-L	G-L	G-L	S-L	Repeat	G-L
SiO_2 (wt.%)	44.56	44.20	44.45	44.30	44.40	43.95	44.60	45.25	44.92	42.90		44.45
TiO_2 (wt.%)	0.11	0.10	0.06	0.15	0.12	0.15	0.16	0.13	0.16	0.08		0.12
Al_2O_3 (wt.%)	2.62	2.84	1.53	3.93	3.40	3.88	4.10	4.65	3.70	1.43		3.41
FeO (wt.%)	8.36	7.91	7.53	8.16	7.84	8.30	7.90	8.17	8.24	10.01		7.92
MnO (wt.%)	0.13							0.15	0.14			
MgO (wt.%)	40.11	41.80	43.75	39.60	39.90	38.95	38.70	36.66	38.08	43.70		39.15
CaO (wt.%)	2.03	2.35	1.40	3.28	3.54	3.04	3.42	3.37	3.45	0.50		2.83
Na_2O (wt.%)	0.17	0.20	0.11	0.30	0.33	0.30	0.36	0.33	0.36	0.11		0.24
Re (ppb)	0.039	0.070	0.025	0.053	0.067	0.025	0.024	0.069	0.026	0.022	0.022	0.016
Os (ppb)	0.831	0.412	0.413	0.979	0.458	0.791	0.889	0.554	0.758	1.90	1.43	0.94
$^{187}Re/^{188}Os$	0.227	0.82	0.29	0.261	0.699	0.152	0.13	0.6	0.168	0.055	0.074	
$^{187}Os/^{188}Os$	0.1222	0.1225	0.1161	0.1303	0.1277	0.1281	0.1265	0.1284	0.1275	0.1150	0.1151	0.1253
Pd (ppb)	2.05	2.19	2.19	2.48	2.36	1.63	2.09	1.96	2.55	0.634	0.870	1.75
Pt (ppb)	3.72	3.52	4.95	3.30	3.59	3.21	3.61	3.02	4.23	2.80	3.32	3.06
Ru (ppb)	4.77	4.33	6.24	6.41	4.13	4.85	6.93	3.48	4.81	7.05	7.08	4.08
Ir (ppb)	3.01	2.53	2.43	3.26	2.46	2.55	2.58	1.70	2.39	3.87	3.88	2.17
S (ppm)		14	6	21	18	14	14	17	16			19

Vitim	314-71	86-1	313-37	313-240	314-580	314-56	314-56
	S-L	S-L	G-L	G-L	G-S-L	S-L	Spinel
SiO_2 (wt.%)	43.61	44.35	45.10	44.53	43.80	44.60	
TiO_2 (wt.%)	0.16	0.15	0.13	0.12	0.17	0.18	
Al_2O_3 (wt.%)	2.05	3.47	3.27	3.23	3.16	4.27	
FeO (wt.%)	8.33	7.86	7.69	8.31	8.80	8.39	
MnO (wt.%)	0.13			0.13			
MgO (wt.%)	41.75	39.95	39.20	41.54	40.27	37.80	
CaO (wt.%)	1.33	3.01	3.45	2.72	2.67	3.89	
Na_2O (wt.%)	0.11	0.33	0.37	0.11	0.29	0.38	
Re (ppb)	0.040	0.043	0.027	0.026	0.036	0.024	0.171
Os (ppb)	0.524	0.719	0.898	0.688	0.998	0.923	0.103
$^{187}Re/^{188}Os$	0.365	0.285286829	0.146	0.178	0.172	0.125	
$^{187}Os/^{188}Os$	0.1174	0.1265	0.1243	0.1252	0.1243	0.1301	
Pd (ppb)	1.30						
Pt (ppb)	1.34						
Ru (ppb)	3.91						
Ir (ppb)	2.39						
S (ppm)	10	17				23	

Namibia	FRB1181	FRB1650	FRB1652	PHN5304	PHN5315	JJG2514	JJG2514	FRB1180	FRB1183	JJG2513	JJG2517	PHN5364
	G-L	G-L	G-L	G-L	G-L	G-L	Repeat	G-L	G-L	G-L	G-L	G-L
SiO_2 (wt.%)	44.4	44.13	43.9	43.28	44.3	44.46		45.75	43.59	45.87	43.55	45.13
TiO_2 (wt.%)	0.02	0.05	0.02	0.14	0.11	0.02		0.02	0.01	0.01	0.01	0.05
Al_2O_3 (wt.%)	0.89	0.61	0.68	1.39	2.05	0.27		0.52	0.63	1.97	1.5	1.5
FeO (wt.%)	7.86	7.64	8.15	10.2	7.56	7.56		7.35	8.54	7.13	7.55	7.61
MnO (wt.%)	0.11	0.12	0.12	0.13	0.13	0.1		0.12	0.1	0.13	0.12	0.11
MgO (wt.%)	45.43	46.21	46.04	43.15	43.57	46.25		45.08	46.08	42.6	45.21	44.87
CaO (wt.%)	0.59	0.57	0.51	1.04	1.49	0.74		0.4	0.41	1.55	1.35	1.01
Na_2O (wt.%)	0.06	0.01	0.01	0.09	0.09	0.08		0.08	0	0.09	0.08	0.09
Re (ppb)	0.058	0.049	0.029	0.319	0.143	0.136	0.130	0.134	0.179	0.337	0.184	0.086
Os (ppb)	5.11	2.49	2.47	5.01	4.75	3.23	3.03	2.70	10.37	2.00	3.02	4.43
$^{187}Re/^{188}Os$	0.076	0.095	0.056	0.263	0.145	0.231	0.207	0.239	0.083	0.813	0.293	0.093
$^{187}Os/^{188}Os$	0.1136	0.1135	0.1168	0.1130	0.1237	0.1179	0.11781	0.1216	0.1139	0.1205	0.1186	0.1150
Pd (ppb)	1.56	0.92	1.18	1.21	3.43	0.64						
Pt (ppb)	5.90	3.14	3.54	2.94	4.85	2.78						
Ru (ppb)	10.02	9.79	9.38	7.69	9.08	4.37						
Ir (ppb)	4.96	3.25	2.54	4.56	3.60	2.81						

Namibia	PHN5365	FRB1625	FRB1651	FRB6199	RAJ 218	RAJ 220	RAJ 221	PHN5465	PHN5510	PHN5790
	G-L	G-L	G-L	G-L	G-L	G-L	G-L	G-L	G-L	G-L
SiO_2 (wt.%)	45.04	44.39	44.83	45.46	44.74	44.57	45.00			
TiO_2 (wt.%)	0.03	0.1	0.08	0.1	0.141	0.075	0.053			
Al_2O_3 (wt.%)	1.5	0.62	0.69	1.14	1.3	1.68	2.34			
FeO (wt.%)	7.61	7.83	7.87	7.61	7.37	8.12	7.87			
MnO (wt.%)	0.14	0.1	0.05	0.09	0.14	0.15	0.15			
MgO (wt.%)	44.09	46.69	46.26	44.57	44.59	42.98	42.23			
CaO (wt.%)	0.79	0.27	0.44	0.99	0.75	1.41	1.76			
Na_2O (wt.%)	0.09	0	0	0.04	0.282	0.41	0.17			
Re (ppb)	0.149	0.456	0.369	0.286	0.506	0.418	0.270	0.309	0.106	0.195
Os (ppb)	1.96	3.89	7.64	7.33	2.42	4.54	3.33	2.22	4.41	7.33
$^{187}Re/^{188}Os$	0.365	0.563	0.232	0.188	1.01	0.443	0.390	0.229	0.213	0.188
$^{187}Os/^{188}Os$	0.1216	0.1166	0.1158	0.1191	0.1234	0.1222	0.1208	0.1143	0.1152	0.1191
Pd (ppb)										
Pt (ppb)										
Ru (ppb)										
Ir (ppb)										

S-L = spinel lherzolite, G-L = garnet lherzolite, S-H = spinel harzburgite, G-H = garnet harzburgite, G-S-L = garnet-spinel lherzolite.
Repeats are repeat dissolutions.
Internal errors on $^{187}Os/^{188}Os$ are all better than 2.0‰.

Table 2
Summary of PGE and Re–Os isotope characteristics

Sample suite	Average		Average		Average		Average		Average		Average		Average		Average	
	Mg number	±	Al_2O_3	±	Os (ppb)	±	$^{187}Re/^{188}Os$	±	$(Os/Ir)_n$	±	$(Pd/Ir)_n$	±	$(Ru/Ir)_n$	±	γ_{Os}	±
N. Lesotho	92.7	1	1.14	0.38	4.2	2.6	0.194	0.177	1.01	0.29	0.192	0.331	1.03	0.38	−12.5	3.1
Somerset Island	92.1	0.3	1.09	0.7	3.6	1.1	0.511	0.905	0.930	0.140	0.445	0.470	1.19	1.34	−11.1	2
Namibia	91.7	0.4	1.21	0.67	4.3	2.3	0.309	0.262	0.980	0.171	0.346	0.226	1.55	0.53	−6.9	2.7
Vitim	89.6	0.7	3.12	1.14	0.84	0.4	0.266	0.221	0.271	0.09	0.645	0.215	1.25	0.22	−2.3	3.9
Beni Bousera[a]	90.6	0.6	2.52	1.14	3.7	0.4	0.211	0.157	1.02	0.03	1.23	0.50	1.2	0.12	−1.9	3
All cratonic					4.2	2.7	0.194	0.274	0.960	0.200	0.435	0.474	1.12	0.43	−11.5	8.8
All off-craton[b]					2.0	1.1			0.710	0.400	1.40	3.12	1.17	0.21	−1.5	3.7
All orogenic					4.0	1.6			1.31	0.59	1.34	0.66	1.32	0.43	−2.5	3.4

Averages for cratonic, non-cratonic and orogenic peridotites taken from the database assembled by Pearson et al. (2003) correct to end 2002.
[a] ID data for this study only. Anomalous Os values for GP91 ans GP220 excluded from means.
[b] Alkali-basalt hosted only.

Namibia xenolith suite probably experienced less melt extraction than the N. Lesotho suite, but still very extensive degrees (25–35%; Fig. 1).

2.4. Vitim peridotite xenoliths

The Vitim peridotite suite was selected from a larger sample collection characterised by Ionov et al. (1993). This suite was collected from a 10–30-Myr-old picritic tuff deposit within the Vitim volcanic field, 200 km east of lake Baikal. The Vitim volcanic field lies within the Baikal rift zone where extension has occurred, presumably on a weak spot, in the Proterozoic lithosphere surrounding the Siberian craton. The samples have been previously characterised for sulfur content (Ionov et al., 1992) bulk rock and mineral chemistry (Ionov et al., 1993; Ionov, 2004), oxygen (Ionov et al., 1994) and Sr–Nd isotopes (Ionov and Jagoutz, 1989). The subset analysed here comprises garnet, garnet–spinel and spinel xenoliths. All facies of these peridotites are coarse grained, with granular, undeformed textures. Equilibration conditions for the xenoliths encompass a P–T range of 850–1200 °C and 1.5–2.5 GPa, equivalent depth range (circa 40–80 km). The lithosphere here is thus considerably shallower than the cratonic Lesotho peridotites or the circum-cratonic Namibian peridotites and has an elevated geotherm, consistent with the rift setting.

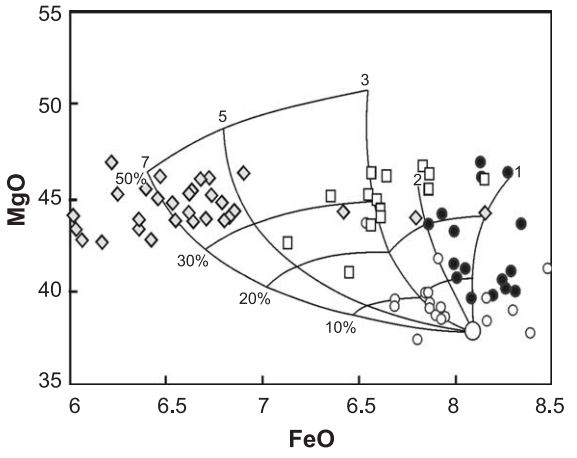

Fig. 1. MgO–FeO relations (anhydrous basis) for Lesotho (diamonds), Namibian (squares), Vitim (open circles) and Beni Bousera (solid circles) peridotites. The melting grid outlines the expected composition of melt residues and is contoured for percentage melt extracted (in 10% intervals) at different melting pressures, in GPa (Walter, 2003). The effect of small amounts of introduced Fe in kimberlite-derived peridotites (e.g., Boyd et al., 1997) results in a small decrease in the apparent pressure of melting and degree of melting.

The Vitim peridotites show a very large range in major-element variation, with Al_2O_3 contents ranging from 1.4 to 4.6 wt.%. Several samples are so rich in Na, Ca and Al that they are more fertile than models of undepleted, fertile mantle compositions. These rocks can have combined garnet and diopside contents up to 25 vol.%. This fertility is also expressed by the Vitim peridotites having the lowest average Mg number of any of the samples analysed (89.6 ± 0.7). FeO–MgO characteristics indicate that the suite have commonly experienced between 5% and 10% melt extraction (Fig. 1). Rare examples, such as 314-6, have high MgO and low FeO and

may have experienced up to 25% melt extraction (Fig. 1). Ca/Al varies widely and may partly reflect diopside and/or garnet introduction during melt interaction.

2.5. Beni Bousera massif peridotites

The Beni Bousera massif is an orogenic peridotite emplaced into the Betic-Rif orogen ~ 22 Myr ago. All our samples were collected at least 1 m from any pyroxenite layering, some from areas where pyroxenite veining was absent or scarce. Six samples from the larger suite studied by Pearson (1989) have been analysed for Re–Os isotopes and PGE (Table 1). Three samples have only Re–Os isotope data. Trace-element data, including whole rock and mineral REE concentrations, are available (Pearson, 1989) and can be obtained from the senior author. Pearson et al. (1993) published Sr and Nd isotopic compositions for these samples. Previous PGE data for the Beni Bousera peridotites have also been presented by Gueddari et al. (1996). However, the Gueddari et al. (1996) data were obtained using non-isotope dilution techniques and a Se–Te collection, fire assay procedure. This technique has been shown to give erratic yields for some PGE due to volatilisation and bead dissolution problems (Gros et al., 2002) and may account for some of the scatter on plots including the Gueddari et al. (1996) data.

Overall, the Beni Bousera sample suite is considerably less depleted in major-element terms than the N. Lesotho and Namibian peridotites (Fig. 1), as reflected by substantially lower olivine Mg numbers (average = 90.6 ± 0.6) and higher average Al_2O_3 contents (2.52 wt.%; Table 2). Major-element systematics are very similar to the peridotites of the geologically similar Ronda massif (Frey et al., 1985) and can be interpreted in terms of their compositions representing residues from varying degrees of melt extraction (Kornprobst, 1969; Pearson, 1989; Gueddari et al., 1996). Estimation of the degree of melt extraction, using the method outlined in Frey et al. (1985) is between 5% and 25% (Pearson, 1989). This corresponds well to estimates based on experimental petrology (Fig. 1) and from REE modelling (Pearson, 1989). Some Beni Bousera samples are anomalously FeO enriched and plot well off the right-hand edge of Fig. 1. This Fe enrichment is likely related to the infiltration of melts that formed the abundant pyroxenite layers (Pearson et al., 1993).

3. Analytical methods

New major-element data presented in Table 1 was obtained using XRF methods described by Boyd and Mertzman (1987) and is taken from Irvine (2002). All Letseng peridotite powders were prepared from a minimum 500 g of coarse crush. PGE analytical protocols followed those of Pearson and Woodland (2000). This methodology allows PGE and Re concentrations and Os isotope composition to be obtained from the same Carius tube sample digestion, thereby minimising the nugget effects to which Os–PGE abundance determinations are so vulnerable. All PGE concentration data are by isotope dilution. Data for Lesotho, Namibia and Vitim xenoliths were taken on a Perkin Elmer Sciex Elan 6000 ICP-MS at Durham using a CETAC Aridus desolvating nebuliser. Beni Bousera Re data were obtained on a Thermo-Finnigan Neptune multi-collector ICP-MS at Durham. All Os concentration measurements were made on totally spiked samples analysed for Os isotope composition via N-TIMS. As such, the internal precision for Os concentration measurements is considerably better than other PGE. This is of little consequence because of the limitations imposed by external factors such as spike calibration and standard stoichiometry issues.

Os isotopic ratios for some Namibian peridotites were determined in a Finnigan MAT-261 mass spectrometer at the Open University. Lesotho and Vitim Os data were taken on the DTM N-TIMS instrument following procedures outlined in Carlson et al. (1999). Some Namibian samples and all the Beni Bousera data presented in Table 1 were obtained at Durham on a Thermo-Finnigan Triton instrument following procedures outlined in Pearson and Nowell (2004). For all these measurements, in-run precision for Os isotope measurements were better than the typical standard reproducibility of 2‰. Reproducibility of duplicate dissolutions represented in Table 1 is equal to or better than this level of precision.

The quality of the PGE data can be assessed using the reproducibility and coherency of data for our in-house Durham University peridotite PGE standard,

GP13, a spinel lherzolite from the Beni Bousera peridotite massif (Table 3). External reproducibility for this standard, expressed as two times the relative standard deviation of the mean was 8.8% Os, 18.4% Ir, 6.7% Ru, 14.9% Pt, 12.6% Pd and 3.3% Re. This standard has also been analysed at a number of other laboratories and a summary of the data obtained by an independent dissolution technique, high-pressure ashing, at the University of Leoben, Austria (Meisel et al., 2001a), by Carius tube at the Danish Lithosphere Centre, and by NiS fire assay and isotope dilution is presented in Table 3. The results are identical to within analytical uncertainty. Small differences are likely due to spike-calibration issues and powder heterogeneity. The relative sense and magnitude of inter-element fractionations for all laboratories are in the same sense relative to chondrites and are within analytical uncertainties.

The variation in concentration data in the Durham standard data set can be interpreted either in terms of analytical deficiencies or in terms of sample heterogeneity. One indication of data quality is the near constancy of the Os/Ir ratio despite varying absolute concentrations. Repeat analysis of this standard gives an Os/Ir value of 1.09 ± 0.06 (1 S.D., $n = 8$), i.e., an overall uncertainty of 10.6% at the 95% confidence level. Repeat dissolution of one of the Vitim samples (314-5a and b; Table 1) gave the following percentage difference in concentration between replicates: Re, Ru and Ir (0–0.4%), Pt (18%), Pd (31%) and Os (28%). Despite relatively poor reproducibility in Os concentrations, the Os isotope ratio is reproducible to within 0.1‰ (Table 1).

Sulfur analytical techniques for the Vitim samples are documented by Ionov et al. (1992). The Lesotho peridotites were analysed for sulfur abundances at the Max-Planck-Institut für Chemie using commercially available apparatus consisting of an induction furnace and infrared-detection system. Approximately 10–50 mg of powder was analysed. Repeat analyses were made for each peridotite using several aliquots to account for heterogeneous sulphide distribution. The accuracy of this method was checked by analysing standards (Dreibus et al., 1995). S abundances spanning those measured in the Lesotho suite are accurate to 10–15%. Below 40 ppm S, accuracy is 20% or above. Detection limit is 10 ppm.

4. Results

Analytical techniques for PGE determination have been rapidly advancing over the last 10 years, and a consensus is being reached that isotope dilution (ID) data is the optimal method of analysis. Recently Morgan et al. (2001) have pointed out potential problems with non-ID Os and Ir determinations by NiS fusion-INA analysis. This, combined with erratic

Table 3
Replicate analyses of the Durham peridotite standard, GP13

Replicate	Os (ppb)	Ir (ppb)	Ru (ppb)	Pt (ppb)	Pd (ppb)	Re (ppb)
Durham data $n = 8$						
Mean	3.87	3.56	6.97	7.00	5.64	0.330
Standard deviation	0.17	0.33	0.23	0.52	0.35	0.010
2 × RSD (%)	8.8	18.4	6.7	14.9	12.6	3.23
Leoben data $n = 3$						
Mean	4.06	3.4	6.05	6.38	5.8	0.312
Standard deviation	0.03	0.08	0.41	0.47	0.16	0.010
2 × RSD (%)	1.5	4.7	13.6	14.8	5.4	6.4
DLC data $n = 9$						
Mean	3.38	6.92	6.43	5.42	0.490	
Standard deviation		0.14	0.75	0.71	0.34	0.190
2 × RSD (%)		8.4	22	11	12.3	78
Chicago data $n = 1$						
	3.60	3.35	7.23	6.15	5.75	

Leoben dissolutions performed by high-pressure ashing (Meisel et al., 2001a,b). DLC = Danish Lithosphere Centre. Data include three dissolutions via high-pressure ashing and three by Carius tube. $n = 6$ for DLC Re data. Chicago data obtained using NiS fire assay ID-ICP-MS (Puchtel and Humayun, 2000).

data produced by non-ID NiS fusion combined with Se–Te collection (Gros et al., 2002), may result in some of the scatter observed on diagrams presented below that combine ID data with older data.

4.1. I-PGE concentrations, correlations and inter-element fractionations

4.1.1. I-PGE concentrations

The Lesotho sample suite has very variable Iridium-Group PGE (I-PGE) abundances. Os varies from < 1 to 13. 7 ppb (Figs. 2 and 3). Ir and Ru are similarly variable (Fig. 2) and range to high levels, but all three elements are well correlated ($R_{(Os/Ir)} = 0.9$; $R_{(Ru/Ir)} = 0.86$). Very elevated concentrations of I-PGE in some samples have been observed previously in cratonic peridotites (Fig. 2; Irvine et al., 2003). Mean values for I-PGE abundances are close to those normally observed in cratonic and circum-cratonic peridotite xenoliths erupted by kimberlites. For instance, the average Os concentration in the Lesotho suite (4.2 ± 2.6 ppb; Fig. 3a; Table 2) is within error of the value obtained for Somerset Island cratonic peridotite xenoliths (3.6 ± 1.1 ppb; Table 2; Irvine et al., 2003) and very similar to the mean Os concentration for Namibian peridotites (4.3 ± 2.3 ppb; Table 2; Fig. 3a). These values are also within error of those typical of orogenic peridotites (4.0 ± 1.6 ppb). The average Os concentration of the small Beni Bousera sample suite is 4.9 ± 4.8 ppb (Fig. 3), slightly higher than the orogenic peridotite average (Table 2). However, this value is heavily influenced by the 17.1 ppb value obtained for GP 91 combined with the relatively small numbers of samples. The average Os content for samples with non-anomalous Os concentrations is 3.8 ± 0.5 ppb (Table 2). Significantly, the global mean Os concentrations for kimberlite-derived cratonic and circum-cratonic xenoliths (4.2 ± 2.7 ppb) is almost identical to that of orogenic peridotites (4.0 ± 1.6 ppb; Table 2; Fig. 3), and these values typify those of

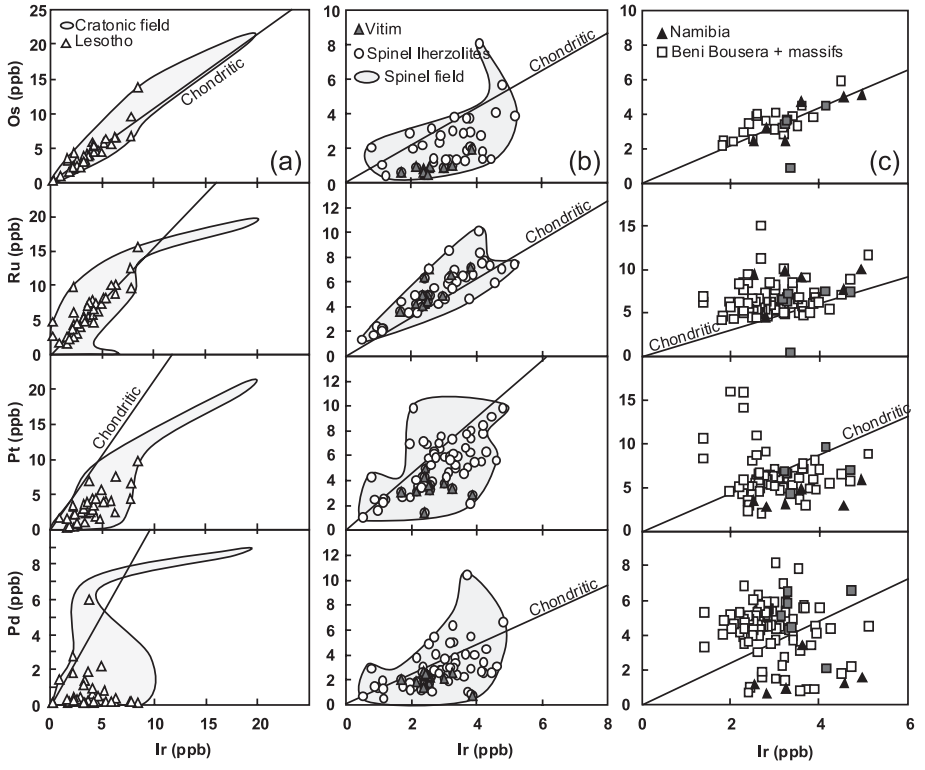

Fig. 2. Covariation of the concentrations (in ppb) of Os, Ru, Pt and Pd with Ir for (a) Lesotho peridotites, (b) Vitim peridotites and (c) Namibian and Beni Bousera peridotites.

residual peridotites. These mean values are higher, although within error of, the value of 3.3 ppb suggested for fertile upper mantle (Morgan, 1986).

In contrast to the other sample suites analysed in this study, the range of Os concentrations of Vitim peridotites is significantly more restricted (Figs. 2 and 3), with the maximum value being well below the average for the other suites. A spinel separate analysed from one Vitim spinel lherzolite (314-56: Table 1) contains relatively low levels of Os (~ 0.1 ppb).

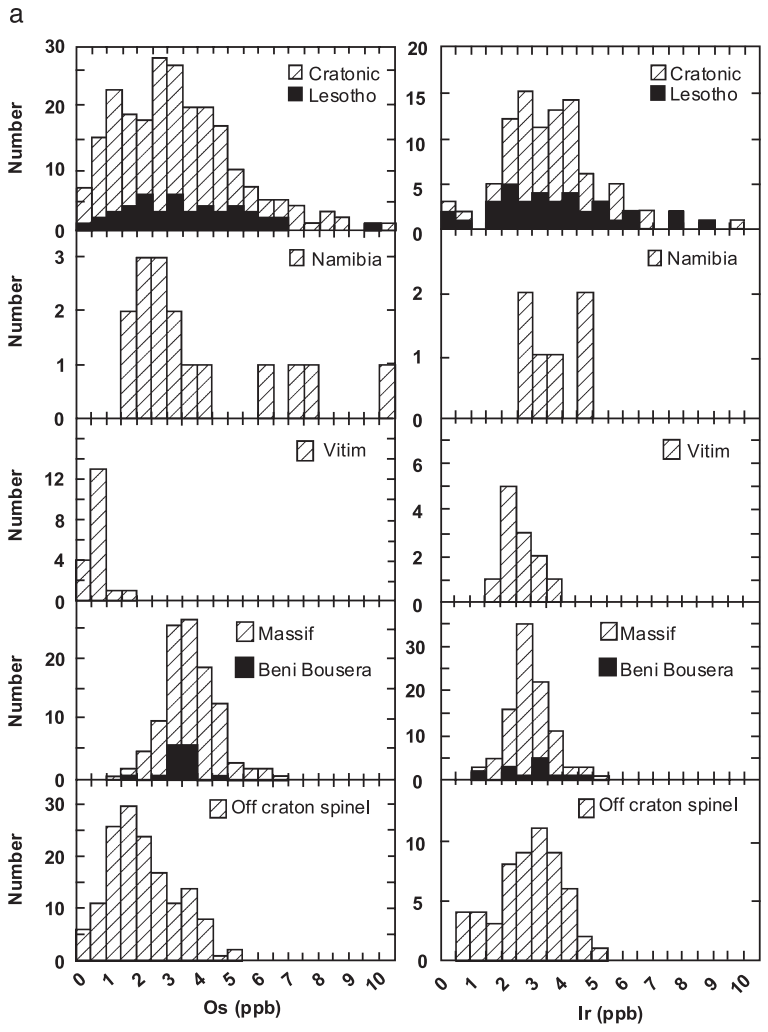

Fig. 3. (a) Frequency distributions for Os and Ir abundances (in ppb) and (b) for chondrite-normalised ratios of Pd/Ir, Ru/Ir and Os/Ir (normalising values after McDonough and Sun, 1995). Data presented for Lesotho, Namibian and Vitim peridotites are from this study (Table 1). Data for Beni Bousera are from this study (Table 1) and from Gueddari et al. (1996). Summary plots for cratonic peridotites comprise data for Lesotho plus peridotite xenoliths from the Jericho kimberlite, N. Slave craton, Canada (Irvine, 2002; Irvine et al., 2003) and from the Somerset Island kimberlite field (J-P pipes and Batty Bay complex; Churchill province; Irvine et al., 2003). Summary plots for orogenic peridotite massifs include data from Beni Bousera plus data from Ronda (Gueddari et al., 1996; Lorand et al., 2000), Lanzo (Lorand et al., 2000) and Pyrenean massifs (Lorand et al., 1999) and Horoman (Rehkämper et al., 1999a,b). Summary plots for off-craton spinel peridotite xenoliths erupted in alkali basalts include data from Rehkämper et al. (1997), Handler and Bennett (1999), Lorand and Alard (2001) and Lee (2002) for PGE data excluding Os. Extra data for Os are taken from literature cited in the review by Pearson et al. (2003). N.B. The Lanzo data of Lorand et al. (1993) was not plotted because of poor agreement of replicates compared with the study of Lorand et al. (2000).

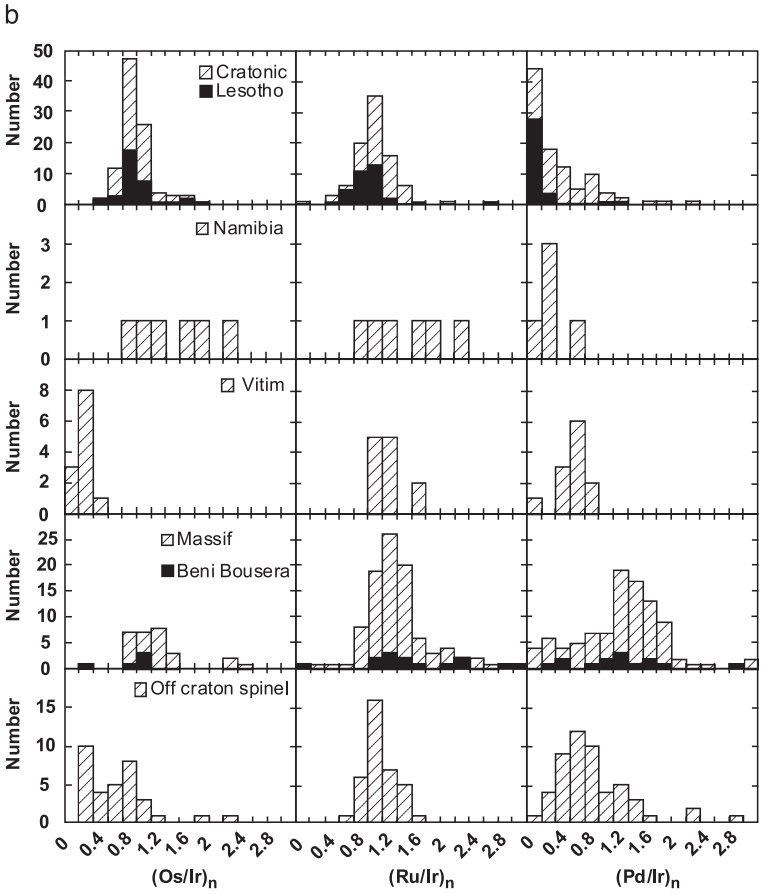

Fig. 3 (*continued*).

Assuming a spinel content of ~ 5% means that only 0.5% of the total Os budget of this rock is contained within the spinel, confirming previous findings that spinel is not an important host for Os in spinel lherzolites (Handler and Bennett, 1999). The low Os abundances in peridotite xenolith spinels contrast with the high Os contents found during experimental studies (Righter and Downs, 2001) or measured in chromite-separates from komatiites (Puchtel and Humayun, 2001). Explanations for this difference may lie in the aluminous nature of the xenolith spinels, the likely presence of sulphide in the Vitim rocks, which may preferentially incorporate most of the Os, and the possibility that the spinel is a break-down product of garnet during lithospheric cooling. Hence, heterogeneous spinel distribution is not a likely cause of the low Os contents of the Vitim peridotites. The validity of the low bulk rock Os concentrations determined in this study are supported by the excellent agreement between our methods and those of Meisel et al. (2001a) using very different dissolution techniques (Table 3) and are confirmed by independent determinations by RNAA (D. Ionov and G. Schmidt, unpublished).

The mean Os concentration for the Vitim sample suite is considerably lower than that of the other sample suites (mean Os = 0.84 ± 0.37 ppb; Fig. 3). Os concentrations lower than the 3.3 ppb fertile mantle average suggested by Morgan (1986) appear to be a general feature of off-craton peridotite xenolith

suites erupted by alkali basalts (Fig. 3). The mean Os concentration of off-craton peridotites worldwide is significantly lower (2.0 ± 1.1 ppb; Table 2) than for cratonic (4.2 ± 2.7) and circum-cratonic peridotites (4.3 ± 2.3) erupted by kimberlites.

4.1.2. Correlation of I-PGE with major elements

Varying degrees of correlation between I-PGE and major elements are observed in the different peridotite suites (Fig. 4). Here, we use Al_2O_3 as an index of melt depletion. We acknowledge that some scatter may be present in the xenolith suites from the metasomatic introduction of diopside. The trends presented in Fig. 4 show the same qualitative variations for other measures of melt depletion such as CaO or Mg number. In the Lesotho suite, there is little correlation between Ir content and Al_2O_3 (Fig. 4), CaO and Mg number (not plotted). A number of samples have Ir abundances in the range of values expected for the residues of high degrees of melting, but there is considerable scatter. The sparse data set for Namibian peridotites is more tightly constrained, although the most depleted samples (lowest Al_2O_3) have both high and low Ir abundances. The Vitim sample suite shows

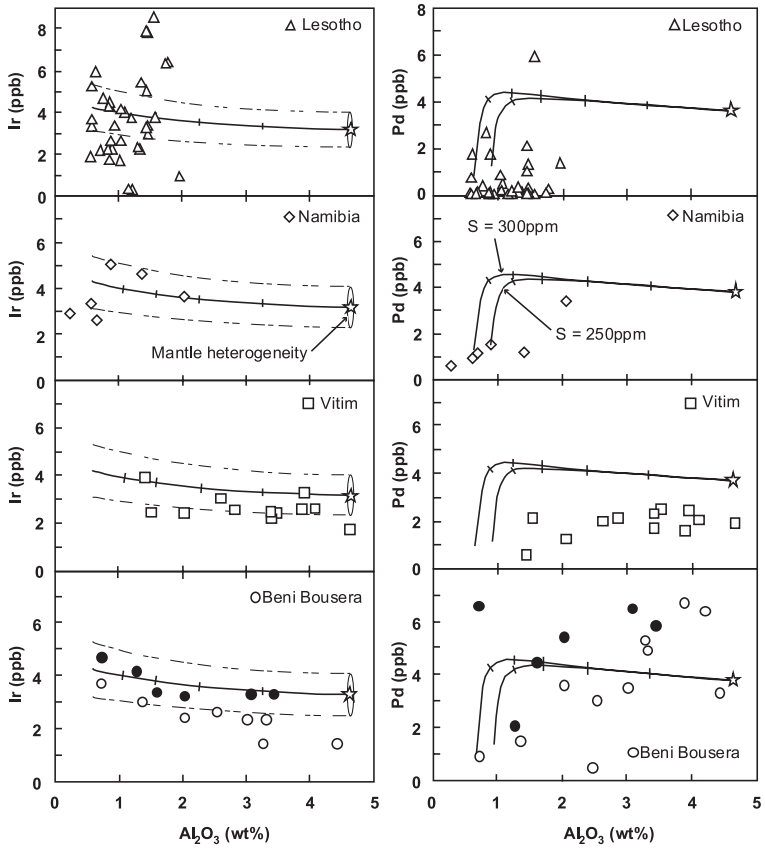

Fig. 4. Variation of Ir and Pd with Al_2O_3 for Lesotho, Namibian, Vitim and Beni Bousera peridotites. Curves model the expected variation of Ir or Pd within a mantle residue experiencing progressive melt extraction. Note the greater coherence of the isotope dilution data (solid circles: this study) to the theoretical melt extraction trend compared to the non-isotope dilution data (open symbols) of Gueddari et al. (1996). Calculations are for non-modal fractional melting using a primitive mantle source (star symbol) containing 250–300 ppm S. The extracted melts have a S capacity of 1000 ppm. A partition coefficient between sulphide and melt, $D_{PGE(sulphide/melt)}$ of 10^4 was selected for Pd following Lorand et al. (1999) and Rehkämper et al. (1999a,b). $D_{Ir(sulphide/melt)}$ was set at 10^5. Tick marks on melt extraction curves indicate 5% melting increments. The two dotted lines paralleling the solid line for Ir melting trends illustrate the effect of increasing or decreasing the primitive mantle Ir content. The two solid trends marked on the Pd melting trends indicate the effect of varying the source S content between 300 and 250 ppm. Varying S content of the source or the S capacity of the extracted melts does not significantly alter the melt extraction trends.

a clearer correlation than the two kimberlite-hosted xenolith suites, largely because of the more extensive range in Al_2O_3 (Fig. 4). Although there appears to be a general increase in Ir as Al_2O_3 decreases, i.e., the mostly depleted sample has the highest Ir content, there is much scatter.

Although the Beni Bousera suite shows a correlation of increasing Ir with decreasing Al_2O_3, as expected for a suite of residues from melt extraction (Fig. 4), the overall trend is too steep to be explained by melt depletion. If the non ID data of Gueddari et al. (1996) are excluded, the data obtained for this study very closely match the theoretical trend of slowly increasing Ir with progressive melt extraction (Fig. 4). The much greater scatter of the non-ID data casts doubt on its validity.

4.1.3. I-PGE inter-element ratios

I-PGE inter-element ratios, e.g., $(Os/Ir)_n$ for both the Lesotho cratonic and Namibian circum-cratonic peridotites remain close to chondritic (Figs. 2 and 3; Table 2). The mean $(Os/Ir)_n$ for Lesotho peridotites is exactly chondritic (1.0 ± 0.3). $(Ru/Ir)_n$ for the Lesotho peridotites scatters a little more than $(Os/Ir)_n$ but if two anomalous samples are excluded from the suite of 35, the average $(Ru/Ir)_n$ value is within 3% of chondritic (1.027). Average $(Ru/Ir)_n$ for the Namibian suite is supra-chondritic but with a high standard deviation (1.55 ± 0.53), i.e., within error of chondrite. The mean $(Ru/Ir)_n$ value for Vitim peridotites is higher than chondritic (1.25 ± 0.22). For the Beni Bousera samples, $(Ru/Ir)_n$ varies between samples analysed by different laboratories. The mean value for samples analysed by Gueddari et al. (1996) is 2.2 ± 0.6, whereas the smaller sample set analysed in this study gives 1.2 ± 0.68. The discrepancy may again relate to the analytical method employed in the earlier study. If only isotope dilution data are considered for samples that do not have anomalous Os contents, $(Os/Ir)_n$ is within error of unity ($1.02 + 0.03$; Table 2).

The low Os concentrations in the Vitim xenoliths are not mirrored by other I-PGE, which are closer, although towards the lower end of the range found in other off-craton xenolith suites (Fig. 3). As a result, $(Os/Ir)_n$ is anomalously low (0.27 ± 0.09). This dramatic fractionation of Os from Ir has been noted in other off-craton, alkali-basalt-hosted peridotite xenolith suites (worldwide mean $(Os/Ir)_n = 0.71 \pm 0.4$; Table 2) and is anomalous compared with xenoliths from kimberlites or orogenic peridotites (Fig. 3).

4.2. P-PGE concentrations, correlations and inter-element fractionations

4.2.1. P-PGE and Re concentrations

P-PGE (Pt and Pd) concentrations are highly variable in all the peridotite suites analysed. Pt forms a general correlation with Ir in most of the suites, but the correlation is much more scattered than those for I-PGE (Fig. 2). Pt concentrations range from those characteristic of fertile mantle ($\sim 0.01 \times$ chondritic) down to very low values (< 0.5 ppb; $< 0.001 \times$ chon-chondritic) and increase to values in excess of 10 ppb in occasional samples (Fig. 2). Pt is most depleted in the Lesotho peridotites, consistent with their origin via the highest degrees of melting.

Pd concentrations are similarly variable and show the least degree of correlation with Ir in all suites (Fig. 2). The Lesotho peridotites consistently have the lowest Pd concentrations, with many samples being less than 0.5 ppb and thus show the poorest correlation between Pd and Ir. This is a feature of cratonic peridotites in general (Fig. 3; Rehkämper et al., 1997; Irvine et al., 2003). Re concentrations in all the samples are mostly less than fertile mantle abundances (0.26 ppb; Morgan, 1986) but vary greatly (< 0.01 to > 0.5 ppb). Abundances in the Lesotho suite vary by two orders of magnitude (Fig. 5). The other peridotite suites show less variation.

4.2.2. Correlation of P-PGE and Re with major elements

Pt and Pd show relatively poor correlations with major-element indices of melt depletion in the Lesotho suite (Fig. 4). Positive correlations of varying degrees exist between Pd and Al_2O_3 for the Namibian suite and the Vitim suite and are consistent with decreasing Pd with progressive melting. The Beni Bousera trend is scattered. The lowest Al_2O_3 sample has the lowest Pd content, but no systematics are evident. Re shows little correlation with major-element indices of melt depletion, both within and between suites. Despite their very depleted major-element characteristics, many Lesotho peridotites have Re abundances similar to, or even higher than the other peridotite suites (Fig. 5).

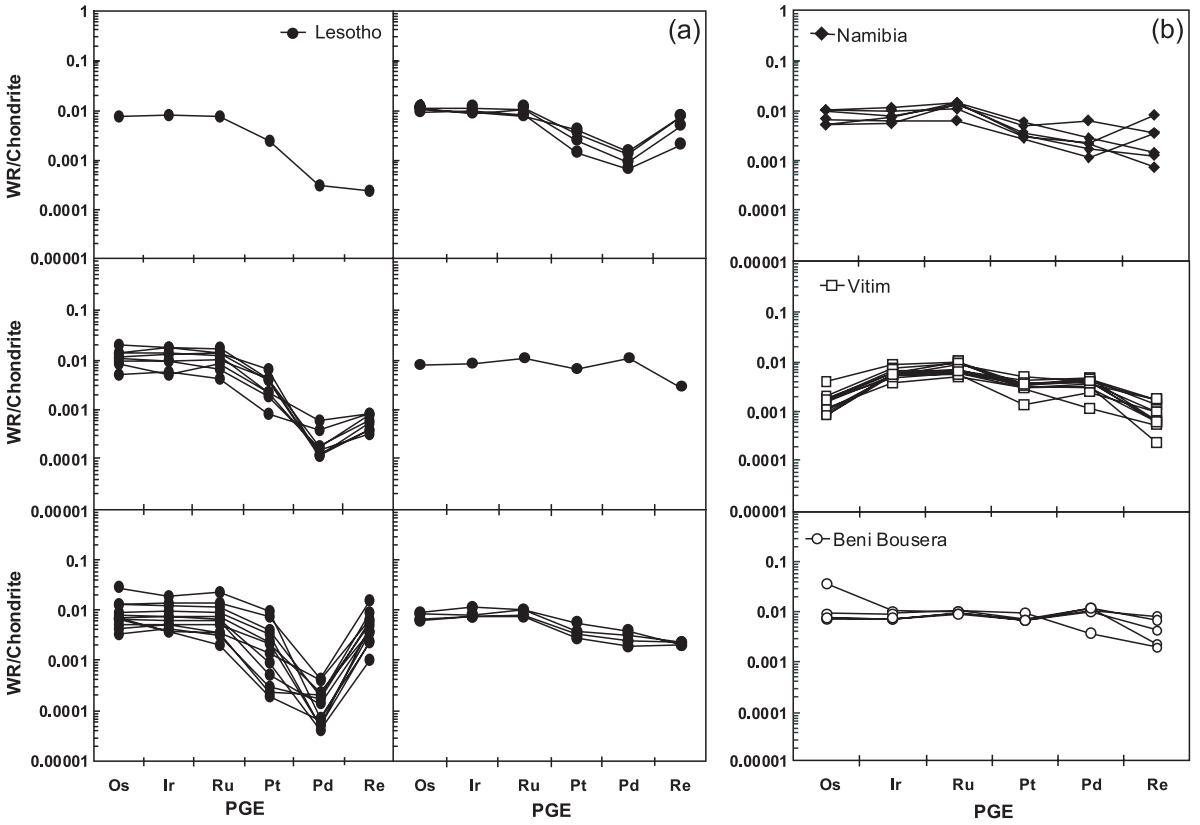

Fig. 5. Chondrite-normalised PGE patterns for (a) Lesotho peridotites and (b) Namibian, Vitim and Beni Bousera peridotites. The different plots group samples on the basis of their PGE patterns, particularly with respect to the different fractionations between Re and P-PGE. Normalising values after McDonough and Sun (1995).

4.3. Fractionation of P-PGE from I-PGE

The fractionation of the less compatible P-PGE plus Re from I-PGE in all the peridotite suites examined is well displayed by their chondrite-normalised PGE patterns (Fig 5). Considerable variation exists in the degree of fractionation of P-PGE from I-PGE in the Lesotho suite. Some Lesotho samples show very marked depletion of Pt (up to two orders of magnitude lower than fertile mantle) and Pd relative to I-PGE. This type of PGE fractionation is characteristic of cratonic peridotites (Rehkämper et al., 1997; Pearson et al., 2002a; Irvine et al., 2003) but has also been observed in mantle rocks from ophiolites (Rehkämper et al., 1997). Pt is depleted relative to I-PGE in the Namibian peridotites but not to the levels observed in the Lesotho suite. The chondrite-normalised ratio of Pd to Ir is a useful measure of the fractionation of P-PGE from I-PGE. The Lesotho peridotites have the lowest $(Pd/Ir)_n$ values of any of the samples analysed. In comparison to cratonic peridotites, the chondrite-normalised PGE patterns of the Namibian, Vitim and Beni Bousera peridotites show much less fractionation of P-PGE from I-PGE (Fig. 5). Mean $(Pd/Ir)_n$ values for the Vitim (0.65 ± 0.22) and Beni Bousera suites (1.3 ± 0.7) are significantly higher than the mean for the Namibian peridotites (Table 2).

$(Pd/Ir)_n$ values for all the peridotites analysed are broadly correlated with major-element depletion (Fig. 6). The most depleted peridotites, with the lowest CaO and Al_2O_3 contents, and highest Mg numbers have the lowest $(Pd/Ir)_n$. This relationship has also been found in other peridotite xenolith suites (Rehkämper et al., 1997; Handler and Ben-

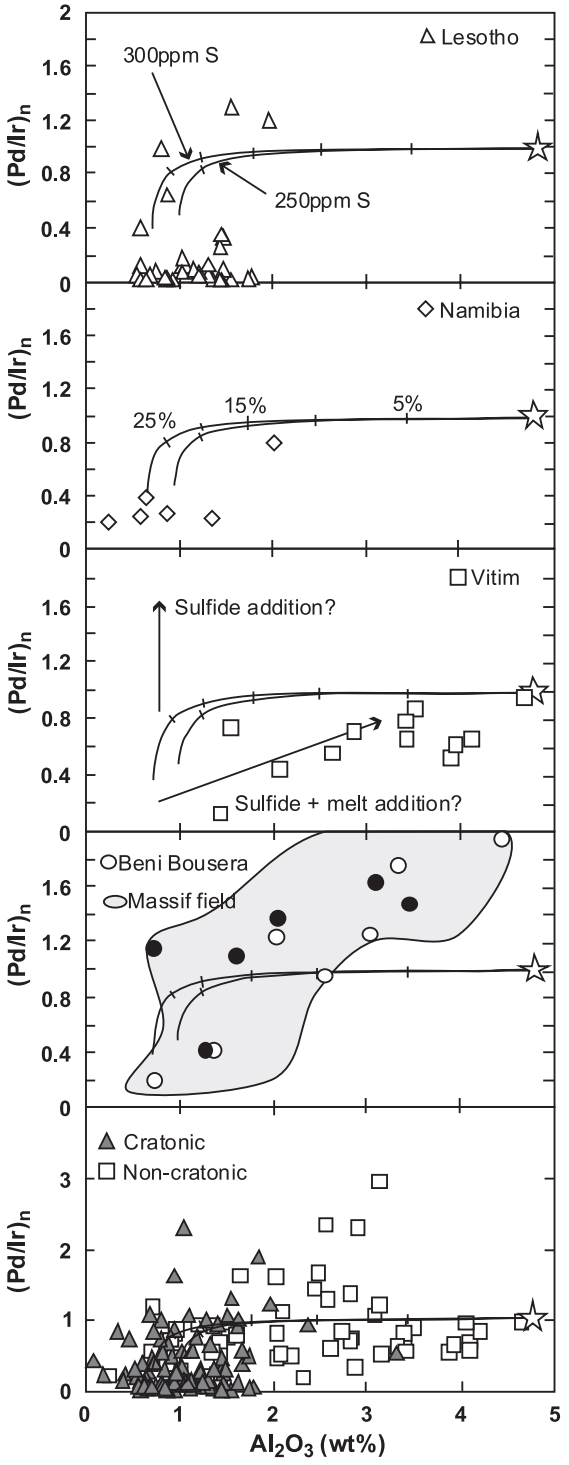

nett, 1999), in orogenic peridotites (Gueddari et al., 1996; Rehkämper et al., 1999a,b; Lorand et al., 1999, 2000) and in abyssal peridotites (Rehkämper et al., 1999a,b; Leguet et al., 2003). In detail, the correlation between these parameters is much stronger for the orogenic peridotites and considerably more scattered for the xenolith suites (Fig. 6), and this may be a function of the addition of diopside to the xenoliths.

Although Re concentrations in most samples are lower than fertile mantle, the majority of xenolith samples show evidence of Re enrichment. For example, on a plot of $(Re/Ir)_n$ vs. $(Pd/Ir)_n$ (not shown), most samples lie on the Re-enriched side of the plot. In addition, Re/Os ratios in whole rock xenoliths are very variable and not well correlated with major-element depletion indices (Fig. 7). In contrast, Re/Os ratios are well correlated with Al_2O_3 contents in the Beni Bousera peridotites (Fig. 7). This is the case for data from other orogenic peridotite massifs (Reisberg and Lorand, 1995).

4.4. Sulfur

Sulfur determinations were made only on the Lesotho suite during this study. These are combined with previously published data for the Vitim suite (Ionov et al., 1992). S abundances in Lesotho peridotites vary widely, from method detection limits to over 350 ppm S (Fig. 8). There is no correlation of S abundance with PGE abundances, and so, it seems unlikely that the variation in S is controlled by melt extraction. This is confirmed by the lack of correlation between S and Al_2O_3 content (Fig. 8). S abundances are similarly variable in the Somerset Island and Jericho cratonic peridotite suites and are interpreted to result from a combination of mantle metasomatism and interaction with crustal fluids

Fig. 6. Correlation of $(Pd/Ir)_n$ versus Al_2O_3 (wt.%) for the Lesotho, Namibian, Vitim and Beni Bousera peridotite suites and a comparison of cratonic and non-cratonic xenoliths. For the Beni Bousera data, solid circles are isotope dilution data (this study), open circles are non-isotope dilution data (Gueddari et al., 1996). Modelling curves illustrate the effect of the extraction of varying degrees of partial melt (in 5% increments of melt fraction) from a fertile peridotite. Modelling parameters as in Fig. 4.

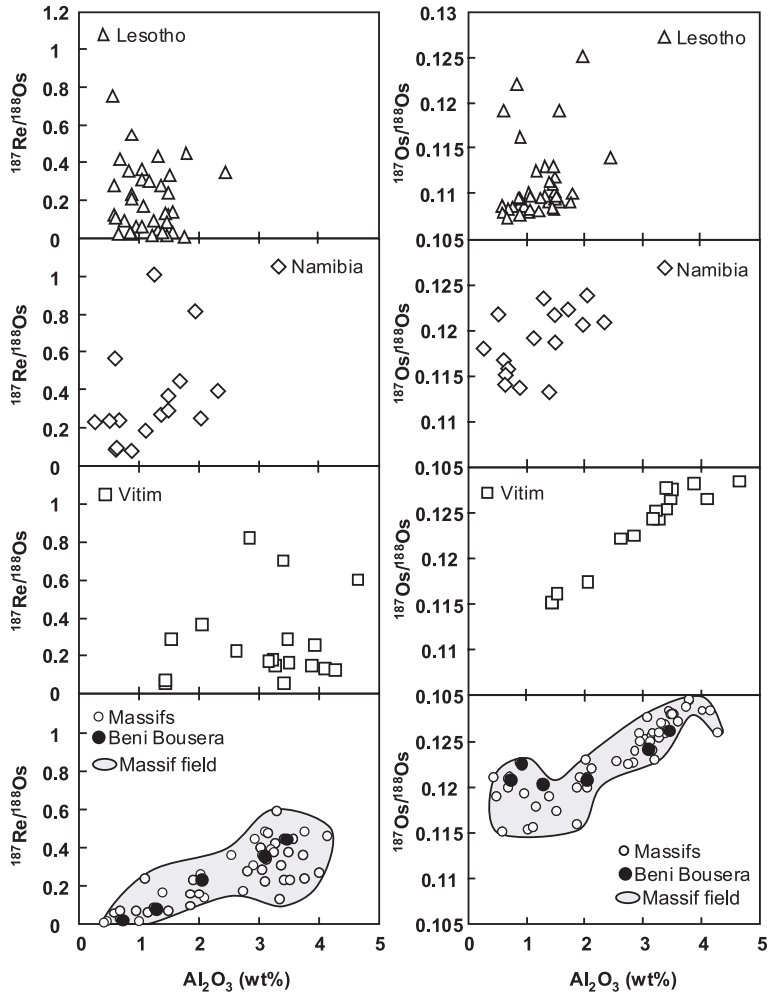

Fig. 7. Covariation of bulk rock $^{187}Re/^{188}Os$ and $^{187}Os/^{188}Os$ with Al_2O_3 contents in Lesotho, Namibian, Vitim and Beni Bousera peridotites. Also plotted is a general field for orogenic peridotites. Data sources for cratonic and off-craton xenolith compilations are summarised in Pearson et al. (2003) and are available from the authors on request. Massif peridotite data is from Reisberg et al. (1991), Reisberg and Lorand (1995), Roy-Barman et al. (1996), Burnham et al. (1998) and Saal et al. (2001). The $^{187}Os/^{188}Os$ with Al_2O_3 correlation for the Vitim suite has an R^2 value of 0.922, a y-intercept of 0.1086 and an intercept at 4.2% Al_2O_3 of 0.12918.

(Irvine et al., 2003). In support of this, elevated S contents (above 150 ppm) are generally associated with high Re/Os ratios.

In contrast to the Lesotho suite, S contents of the Vitim peridotites are all less than 50 ppm (Fig. 8). Although the low S values cluster at low Pd, the lack of covariation of S with Ir or Al_2O_3 (Fig. 8) suggests that melt depletion processes are not the main factor responsible. The very low, sub-chondritic $(Os/Ir)_n$ values for Vitim peridotite xenoliths are associated with very low S abundances compared to lherzolites from orogenic massifs that have similar levels of major-element depletion.

4.5. Re–Os isotopes

4.5.1. Lesotho peridotite

In general, the Lesotho peridotites are characterised by very unradiogenic $^{187}Os/^{188}Os$ (Irvine et al., 2001; Fig. 9). The range and mode match those of the main

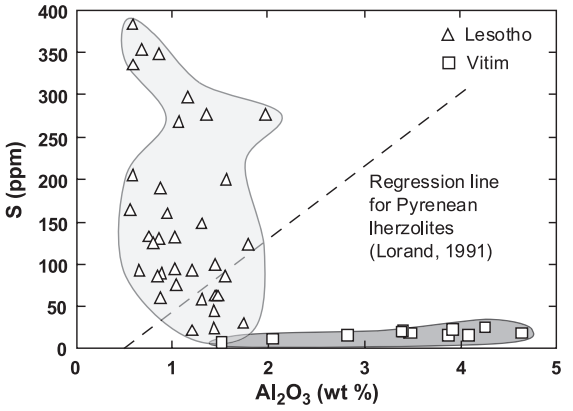

Fig. 8. Covariation between bulk rock S and Al_2O_3 content for the Lesotho and Vitim peridotite xenolith suites. Also shown is the regression line for the Pyrenean orogenic peridotites from Lorand (1991).

population of Kaapvaal peridotites analysed previously (Pearson et al., 1995; Carlson et al., 1999). The least radiogenic Os isotope compositions extend to γ_{Os} values of -18. A very pronounced peak in γ_{Os} values appears between -13 and -15, with a tail stretching towards more positive values.

Lesotho peridotites show poor correlation between Re/Os or Os isotopic composition and indices of melt depletion (Fig. 7). This is characteristic of cratonic peridotites in general (Carlson et al., 1999; Meisel et al., 2001a,b; Pearson et al., 2002a). In contrast, Os isotopic composition shows a good positive correlation with $(Pd/Ir)_n$ (Fig. 10) from very low $(Pd/Ir)_n$ values (0–0.15) at low γ_{Os} (-13 and -16) to $(Pd/Ir)_n$ values in excess of chondritic at slightly sub-chondritic γ_{Os}.

4.5.2. Namibian peridotites

This suite of peridotites is also characterised by exclusively sub-chondritic γ_{Os} values, ranging from -2 to -11 (Fig. 9), but no prominent mode in the distribution is evident. The least radiogenic γ_{Os} values (-11) are significantly higher than the prominent mode in γ_{Os} values of -13 to -15 that characterises cratonic peridotites. The Namibian peridotite also show little correlation between Re/

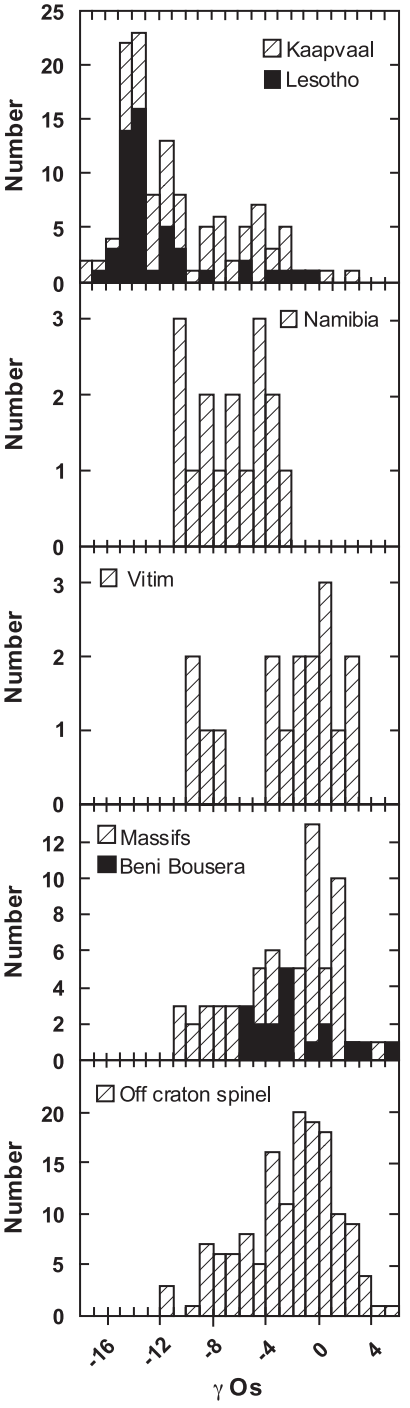

Fig. 9. Frequency distribution of γ_{Os} values for the Lesotho, Namibian, Vitim and Beni Bousera peridotite suites and a comparison of cratonic and non-cratonic xenoliths. Data sources as for Fig. 7. γ_{Os} values for massifs calculated at the time of their crustal emplacement. γ_{Os} values for xenoliths calculated at the time of their eruption.

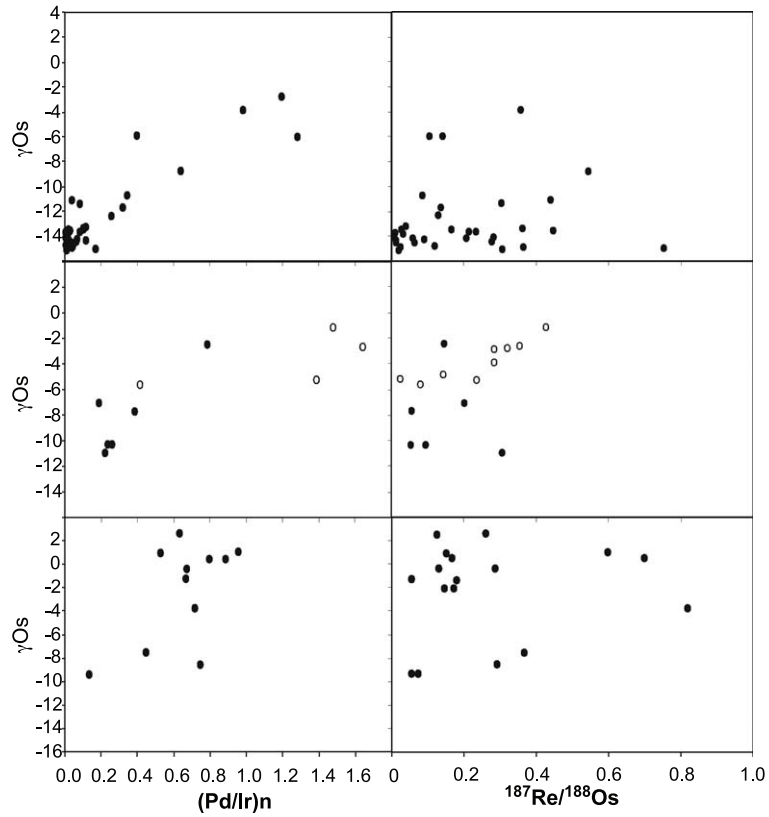

Fig. 10. γ_{Os} versus $(Pd/Ir)_n$ and $^{187}Re/^{188}Os$ for Lesotho, Namibian, Beni Bousera and Vitim peridotites. In the panel that contains the Namibian and Beni Bousera data, the Namibian peridotites are the solid circles, and Beni Bousera samples are open circles.

Os ratio or Os isotopic ratio and bulk rock Al_2O_3 (Fig. 7), but $(Pd/Ir)_n$ shows a broad correlation with γ_{Os}.

4.5.3. Vitim peridotites

This suite has a similar range of γ_{Os} values to the Namibian suite, with two samples as low as −9. There is no pronounced mode (Fig. 9). Several samples have slightly supra-chondritic γ_{Os} values. The overall range is similar to the global compilation of off-craton spinel peridotite xenoliths (Fig. 9). The Vitim suite shows considerable scatter on plots of γ_{Os} vs. either $(Pd/Ir)_n$ or Re/Os ratio (Fig. 10). Although the relationships are complex, the sample with the lowest $(Pd/Ir)_n$ has the lowest γ_{Os} value, indicating that this sample is the least disturbed by metasomatic agents that may have affected Os isotope systematics. In contrast to the scattered relationships shown by Re/Os and Pd/Ir with γ_{Os}, Vitim samples show the best positive correlation between $^{187}Os/^{188}Os$ and bulk rock Al_2O_3 so far recorded for a suite of peridotites ($R^2 = 0.92$; Fig. 7). The intersect of this trend at 4.2% Al_2O_3 at $^{187}Os/^{188}Os = 0.1292$ is within error of Meisel et al.'s (2001a,b) estimate of primitive upper mantle defined from similar trends in xenoliths and massif peridotite suites.

4.5.4. Beni Bousera peridotites

This suite shows a more restricted range of Os isotope compositions ($\gamma_{Os} = -0.49$ to -5.1) compared to the other sample suites and to the Pyrenean and Horoman massifs (Reisberg and Lorand, 1995; Saal et al., 2001; Fig. 9). Although the database is small, both $(Pd/Ir)_n$ and Re/Os show scattered positive correlations with γ_{Os} (Fig. 10). Compared to the

xenolith suites, Re/Os shows a good positive correlation that degrades at low Re/Os. The $(Pd/Ir)_n$ correlation is not as pronounced. Supra-chondritic $(Pd/Ir)_n$ (>1.2) is observed for samples with γ_{Os} ranging from −5 to −1. A combination of the Os isotope data set of Reisberg and Lorand (1995) with the PGE data set of Lorand et al. (1999) gives an excellent correlation between $(Pd/Ir)_n$ and $^{187}Os/^{188}Os$ ($R^2 = 0.90$) for Pyrenean massifs. Beni Bousera peridotites show a good correlation of Os isotope composition with bulk rock Al_2O_3 (Fig. 7), as found previously for other massif peridotites (Reisberg and Lorand, 1995; Saal et al., 2001).

5. Discussion

5.1. Elemental variations and PGE fractionations

5.1.1. Effects of partial melting

PGE in fertile, unmelted mantle predominantly reside in base metal sulphides (e.g., Jagoutz et al., 1979; Mitchell and Keays, 1981), and this is supported by positive correlations between bulk rock PGE content, Cu and Se (Lorand et al., 1999; Handler and Bennett, 1999; Lorand and Alard, 2001). Experiments and observation indicate that monosulphide solid solution (Mss) preferentially accommodates refractory PGE (Os, Ir, Ru, Rh) during melting, relative to Cu-sulphides, which concentrate Pd and Re (Lorand and Alard, 2001; Pearson et al., 1998). For low to moderate degrees of melting (<15%), residual sulphides can be shown to buffer PGE abundances in mantle peridotite to relatively constant levels because of the high $D^{sulphide/melt}$ (e.g., Lorand et al., 1999). At the higher degrees of melting (>25%) experienced by the cratonic peridotites, low-melting point sulphides are consumed (Figs 4 and 6). P-PGEs and Re quantitatively partition into the melt phase during high degrees of melting (>30%), probably due to the breakdown of the Mss. In contrast, the higher melting point (I-PGE) remains in the residue and may be stabilised in either alloy phases or high melting point residual Ru–Os–Ir sulphides (Brenan and Andrews, 2001). This produces a highly P-PGE-depleted residual peridotite with a highly fractionated chondrite-normalised PGE pattern.

This scenario is supported by the observation that many of the Lesotho peridotites have extremely P-PGE-depleted patterns (Fig. 5), with very low Pd and Pt abundances and low $(Pd/Ir)_n$, frequently <0.1. This is consistent with their major-element characteristics that indicate >40% melt extraction (Fig. 1). Mean $(Pd/Ir)_n$ for the Namibian suite is higher (0.35 ± 0.23) than the Lesotho suite (0.19 ± 0.33; Table 2), consistent with their lower levels of melt depletion (20–30%; Fig. 1). The most P-PGE-depleted Namibian peridotites sit close to the end-point of the theoretical melting trends in Fig. 4. On the basis of their relative depletion in Pd and $(Pd/Ir)_n$ fractionation, these peridotites appear to represent residues that have lost enough melt fraction to almost, but not quite consume Mss, in agreement their MgO–FeO systematics. The depletion of Pd and fractionation of Pd from Ir in the Vitim and Beni Bousera suites is more complex and likely significantly affected by later melt interaction.

The PGE fractionations observed over a wide range of melt extraction allow us to comment on the likely hosts for PGE in depleted mantle residues. The coherency of the Ru/Ir and Os/Ir relationships in Lesotho and Namibian peridotites (Table 2; (Figs. 2, 3b and 11)) suggest that these elements are controlled by same phase. Ru/Ir and Os/Ir in the Lesotho suite are constant over a very large range of Pd/Ir (Fig. 11), implying that a phase with a very high partition coefficient for these elements was stabilized during the melt extraction process. These data further imply that the variations observed in Os/Ir and Ru/Ir in other peridotite suites are unlikely to be due solely to the partial melting process as suggested by some authors (e.g., Rehkämper et al., 1997).

The highly fractionated Lesotho bulk rock PGE patterns (Fig. 5) and the lack of correlation between Pt and Ir (Fig. 2) clearly show that Pt is fractionated from I-PGE during extraction of melt. Hence, even if Pt-rich micro-alloy phases are stabilized during the early stages of melt extraction via incongruent melting of metal sulphide complexes (e.g., Lorand et al., 1999), after extensive (>30%) melt extraction, any such alloys began to partition Pt into the extracted melt. Data from the residues of large degrees of melting studied by us confirm the relative partitioning behaviour of most PGE

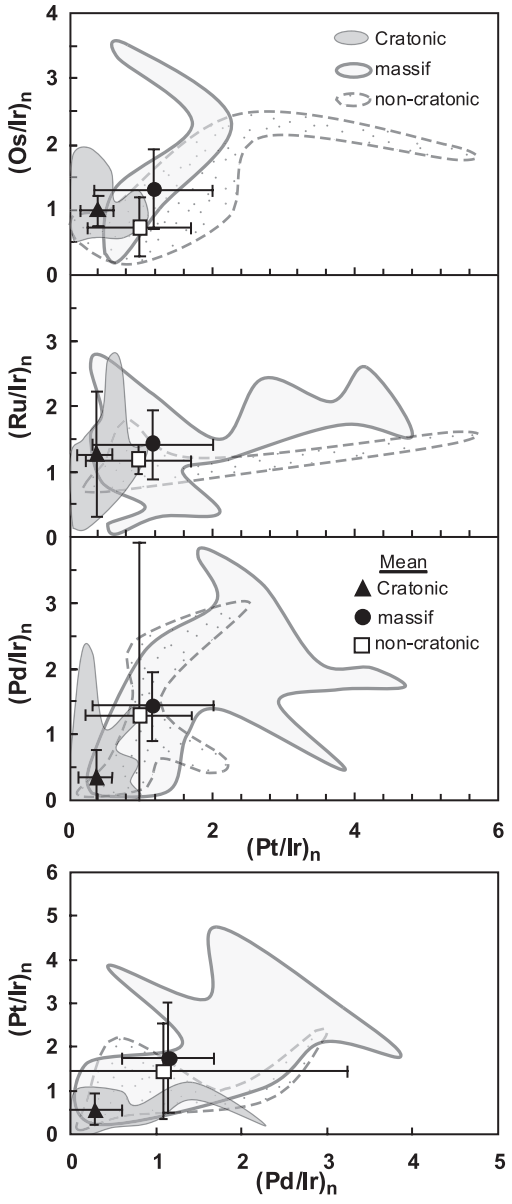

Fig. 11. PGE interelement fractionation plots. Fields for global cratonic and non-cratonic peridotite xenoliths and massif peridotites indicated. Also shown are mean values plus one standard deviation for these categories. Data sources and normalising values as in Fig. 3.

during melt extraction suggested by studies of less depleted peridotites (e.g., Handler and Bennett, 1999; Lorand et al., 1999). However, our data give a clear indication of the incompatibility of Pt at high degrees of melt extraction compared to I-PGE. The relative order of PGE compatibility during mantle melting indicated by our data is thus:

$$D^{Os}_{solid/melt} \sim D^{Ir}_{solid/melt} \sim D^{Ru}_{solid/melt} > D^{Pt}_{solid/melt} > D^{Pd}_{solid/melt} > D^{Re}_{solid/melt}$$

5.1.2. I-PGE abundance variability and Os/Ir fractionation

The Beni Bousera and Vitim peridotite suite show a greater overall variation in bulk rock Al_2O_3 contents and are thus potentially more useful for evaluating the accuracy of the melt modelling presented in Fig. 4, provided that melting is the dominant process affecting PGE systematics. Trends for Ir vs. Al_2O_3 in both suites are subparallel to the model melt depletion trends. When only ID data are considered for Beni Bousera, the limited data provide an excellent fit to the expected melt depletion trend. The trend for the Vitim suite is offset towards the lower range of fertile mantle Ir starting contents. The general approximation of the data to the calculated melting trends indicates that the selection of sulphide-melt partition coefficients was reasonably appropriate. Namibian peridotites plot along an extension of the trends for Beni Bousera and Vitim (Fig. 4). In contrast, the variation in Ir abundances in the Lesotho suite shows considerable scatter at a more restricted range of Al_2O_3. This extreme variation in Ir (and Os) contents is too large to account for by partial melting unless random variations in the sulphide-melt partition coefficients of many orders of magnitude is invoked. The excellent correlation of Ir (and Ru) with Os (Fig. 2a) indicates that this variation is not due to analytical error. One possible explanation is that at very high degrees of melting, I-PGE partition into micro-alloy phases that become very heterogeneously distributed in the host rock. Hence, the variability might represent a sampling error related to the very heterogeneous distribution of high I-PGE phases combined with the limited sampling scale of individual xenoliths. Another possibility is that the variability could be the result of mobilization of Ir and Os by hydrothermal fluids. This is not favoured by the coherent variation of Ir, Ru and Os, which might be expected to have very different behaviour in hydrothermal fluids (Wood,

1987). Some of the variability in Ir (and Os) concentrations may also result from I-PGE loss due to S-undersaturated melt percolation in some samples (e.g., Rehkämper et al., 1999a) combined with reprecipitation of these high I-PGE fluids or sulphide melts, as metasomatic sulphides in the high Ir–Os samples. Detailed combined studies of sulphides and whole rocks in peridotites should resolve these possibilities.

One striking feature to emerge from the preponderance of high-quality Re and Os abundance data resulting from Re–Os isotope work on xenoliths is that the mean Os concentration for any suite of cratonic peridotite xenoliths (global mean = 4.2 ± 2.7 2.7 ppb; Table 2) is always higher than that for suites of non-cratonic peridotites erupted by alkali basalts (spinel and garnet facies; 2.0 ± 1.1 ppb). Because Os is compatible, residues from large degrees of melting should have higher Os than PUM. This is the case for cratonic peridotites. Off-craton peridotites are also residual, yet they have significantly lower Os than PUM, with numerous samples having concentrations below 1 ppb. The Vitim peridotites are an extreme example of this phenomenon (mean Os 0.84 ± 0.4 ppb). Ir contents are not as low. The resulting low Os/Ir are unlikely to be due to "nugget" effects because all Ir and Os data presented here were obtained from the same sample dissolution. Despite the Namibian peridotite suite being non-cratonic, the mean Os abundance of this suite is very similar to the cratonic peridotites (Table 2). Furthermore, massif peridotites such as Beni Bousera generally have mean Os contents very similar to those of cratonic, kimberlite-derived peridotites. The low Os contents in other off-craton, alkali-basalt-borne peridotites are also not matched by correspondingly low Ir contents, leading to anomalously low $(Os/Ir)_n$ ratios (e.g., Handler et al., 1999; Lee, 2002). Although the global mean $(Os/Ir)_n$ for these peridotites (0.71 ± 0.4) is not as low as the Vitim suite (0.27 ± 0.9), they are significantly lower than the chondritic values displayed by kimberlite-borne peridotites and massifs.

Melt percolation through peridotites can dissolve residual sulphides (e.g., Lorand and Alard, 2001; Lorand et al., 2003; Luguet et al., 2003) and hence lower Os. This process may be more prevalent in the off-craton suites studied so far compared with cratonic peridotites, although this seems doubtful given the evidence for interaction of cratonic xenoliths with melt (e.g., Kelemen et al., 1998; Simon et al., 2003). Massif peridotites represent a similar range of melt extraction to off-craton peridotite xenoliths (e.g., Fig. 1); hence, it seems likely that Os should be hosted in similar phases. Hence, any explanation whereby the Os in off-craton peridotite xenoliths is more susceptible to weathering must account for the similar, variable degrees of serpentinisation and weathering of massifs and xenoliths. Handler et al. (1999) prefer an explanation linked to late-stage Os loss due to breakdown of Mss during rapid eruption of xenolith suites and subsequent Os loss due to alteration. This might explain the relative difference between the mean Os contents in off-craton xenoliths and massif peridotites, but some modification is required to explain why kimberlite-derived xenoliths that are transported to the surface even more rapidly that alkali-basalt-borne xenoliths are not susceptible to the same processes. The chondritic Os/Ir in kimberlite-borne peridotites might be due to a combination of (a) Os residence in less readily altered micro-sulphide and alloy phases that do not break down during eruption and (b) a possibly less oxidising environment during the eruption of kimberlites. The very low S content of the Vitim peridotite xenoliths is surprising given their fertile nature (Fig. 8) and indicates S-loss due to sulphide weathering. This may also account for the very low Re abundances in Vitim peridotites, despite their high level of fertility. Currently, explanation of the low Os/Ir values observed in off-craton, alkali-basalt-borne xenoliths appears weighted in favour of them being affected by secondary alteration of Mss decomposed during eruption (Handler et al., 1999).

5.1.3. Inter-elemental PGE fractionation, Os isotope variation and mantle metasomatism

As found in previous PGE studies of peridotite xenolith suites (Handler and Bennett, 1999; Lorand and Alard, 2001), there is little correlation between degree of metasomatic enrichment of lithophile elements and enrichment of PGE in our xenolith suites. For instance, there is no correlation between degree of light rare-earth element (LREE) enrichment and P-PGE enrichment (not plotted). The Lesotho cratonic peridotite xenoliths show ubiquitous LREE enrich-

ment (Irvine, 2002), yet all samples show sub-chondritic $(Pd/Ir)_n$ that must, at least in part, reflect their melt-depletion history.

Despite this, various aspects of the PGE geochemistry of the peridotite xenoliths and massif peridotites are likely attributable to metasomatic effects that involve the introduction of sulphide, probably accompanied by silicate melt. Modelling of melt reenrichment involving the addition of new sulphides to variably depleted melt residues during magma–solid interaction produces elevation of the $(Pd/Ir)_n$ ratio to supra-chondritic levels and elevated P-PGE contents (Rehkämper et al., 1999a,b), and these effects have been well documented in xenoliths (e.g., Lorand et al., 2003) and abyssal peridotites (Rehkämper et al., 1999a; Luguet et al., 2003). In addition, such interaction produces correlations between Os isotopic composition and $(Pd/Ir)_n$ (e.g., Lee, 2002).

A strong correlation between Os isotopic composition and $(Pd/Ir)_n$ is observed for the Lesotho xenolith suite. Supra-chondritic $(Pd/Ir)_n$ values are accompanied by sub-chondritic γ_{Os} values, suggesting relatively recent interaction with a metasomatic component (Fig. 10). The correlation is not as evident for Re/Os vs. γ_{Os}, possibly because of either decoupling between Re and Pd enrichments and/or the greater mobility of Re due to crustal alteration (e.g., Handler and Bennett, 1999).

$(Pd/Ir)_n$ is not well correlated with Os isotopic composition in the Vitim suite. A shallow trend exists for $(Pd/Ir)_n$ vs. Al_2O_3 (Fig. 6) that is too shallow to be explained in terms of partial melting. Such trends can be explained in terms of melt + sulphide addition (Fig. 6), where Al (and probably Ca) is being introduced by the melt and Pd is introduced by the sulphide component. The melt introduction may be responsible for the widely varying, non-chondritic Ca/Al of the Vitim suite. The Lesotho peridotites show almost two orders of magnitude variation in $(Pd/Ir)_n$ at almost constant bulk rock Al_2O_3. This variation is unlikely to be due to melt depletion and is compatible with the addition of Pd by crystallisation of Pd-enriched secondary Cu-rich sulphides (e.g., Rehkämper et al., 1999a; Alard et al., 2000). This variation is superimposed on a marked variation in Al_2O_3 at low levels of Pd and low $(Pd/Ir)_n$ values. Hence, an additional metasomatic process may disturb Al_2O_3 while producing little effect on P-PGE systematics.

The Beni Bousera peridotites have supra-chondritic $(Pd/Ir)_n$, by up to 60%, at sub-chondritic γ_{Os} values. Elevated $(Pd/Ir)_n$ values, along with supra-chondritic Ru/Ir and Rh/Ir in massif peridotites have been explained as an intrinsic source feature that is a characteristic of this type of subcontinental mantle (e.g., Pattou et al., 1996; Lorand et al., 1999; Lorand et al., 2000). If this fractionation is a source feature, there should be no reason to expect correlation between $(Pd/Ir)_n$ and bulk Al_2O_3, especially at >1.5 wt.% Al_2O_3 where little Pd/Ir fractionation is expected from partial melting effects (Fig. 6). However, a strong positive correlation between $(Pd/Ir)_n$ and Al_2O_3 is observed for Beni Bousera and for all massifs, that is more readily interpreted in terms of addition of sulphide by a sulfur-saturated melt (e.g., Rehkämper et al., 1999a). This interpretation is further supported by a similar positive correlation between $(Ru/Ir)_n$ and bulk rock Al_2O_3 content (not plotted). Although the mean $(Ru/Ir)_n$, $(Pt/Ir)_n$ and $(Pd/Ir)_n$ values for massif peridotites are higher than cratonic and non-cratonic peridotite xenoliths (Fig. 11), the global data set for massifs shows considerable scatter. The tightly clustered, close to chondritic Os/Ir and Ru/Ir values of cratonic peridotites plus the chondritic Ru/Ir values of non-cratonic peridotite xenoliths combine to form a large data set (Table 2; Fig. 11) indicating that the subcontinental lithosphere is not elevated in these elemental ratios. The contrasting supra-chondritic and widely varying Ru/Ir, Pt/Ir and Pd/Ir in massif peridotites (Fig. 11) that covary with bulk rock Al_2O_3 are thus most simply interpreted as the effects of melt–solid interaction, as suggested by Rehkämper et al. (1999a). These data increase the documentary evidence for the modifying effects produced by porous melt flow on the PGE systematics of lithospheric mantle (Lorand et al., 2003; Luguet et al., 2003).

5.2. The timing of PGE fractionation: using PGE systematics to evaluate Os model ages

5.2.1. Lesotho peridotite xenoliths

The complex and varied nature of the Lesotho whole rock PGE patterns (Fig. 5) illustrates the problem of using a conventional Re–Os model age approach (T_{MA}) to calculate ages, where the system is assumed to be closed. Variable whole rock Re/Os, uncorrelated with depletion indices, reflects a variety

of metasomatic effects that have long been documented (Pearson et al., 1995; Carlson et al., 1999). In situ sulphide studies have found multiple generations of sulphides in mantle peridotites that affect their PGE patterns (Alard et al., 2000; Luguet et al., 2001; Lorand and Alard, 2001) and their Re–Os isotope systematics (Griffin et al., 2002; Alard et al., 2002). Whole rock analyses integrate these multiple generations of sulphides, and this accounts for the spectrum of ages recognised by Pearson et al. (1995) and Carlson et al. (1999). Because metasomatic sulphides are high in Re and P-PGEs (e.g., Alard et al., 2000; Lorand and Alard, 2001) then the incompatible P-PGEs and Re can be severely disturbed. Metasomatic sulphides can also contain between 1 and 10 ppm Os, and hence, 0.1% or more sulphide introduction can potentially disturb both the Os abundance and Os isotope ratio of the host peridotite. Thus, Re depletion (T_{RD}) and Re–Os model ages (T_{MA}) will also be sensitive to metasomatic sulphide addition. Although a powerful technique, in situ measurement techniques for sulphides are relatively imprecise at the current time, such that internal errors are a factor of 10–100 greater than whole rock analyses (between 2% and >10% for many sulphides in xenoliths; Alard et al., 2002). Much higher precision data can be obtained, even on very low Os sulphides (<50 ppb) such as those found in eclogites, using single-grain micro-chemistry techniques and N-TIMS analysis (Pearson and Spetsius, in preparation). An additional complication of sulphide analyses in mantle peridotites lies in whether to interpret the isotopic information that they provide as reflecting the age of lithosphere differentiation or some prior melting event (see below).

Most cratonic peridotites are residues of very large degrees of melting (>40% e.g., Fig. 1). Modelling (e.g., Barnes et al., 1985; Fig. 6) indicates that removal of ≫30% partial melt from a peridotite is likely to remove the primary Mss due to incorporation of all sulphide into the melt. Brenan and Andrews (2001) have suggested that Mss in a peridotite undergoing extensive melt extraction may breakdown to micro-sulphides such as laurite, or to an Ru–Ir–Os alloy phase, with much higher solidi than Mss. Mss grains that are residues of very high degrees of melting therefore should not exist due to depletion of sulfur in the residue. Some Mss with "residual" PGE characteristics are found in olivine grains from kimberlite mine concentrate and also by serial sectioning of xenoliths (e.g., Pearson et al., 2002a; Griffin et al., 2002). However, it is possible that these sulphides are "secondary" because a highly depleted residue should not contain Mss. In some xenoliths, these enclosed Mss grains have less radiogenic Os isotope compositions than the whole rocks. In others, the large analytical uncertainties on the sulphide values are within error of the whole rock values. Analyses of high Os, low Re/Os and low Pd/Os sulphides in Lesotho xenoliths (Griffin et al., 2002) give Re–Os model ages that are as old, within 2σ error, as the oldest bulk rock Re depletion ages published for these xenoliths (e.g., Pearson et al., 1995). This is also the case for Siberian lithospheric peridotites, where the oldest whole-rock depletion ages for xenoliths are within error of the oldest ages calculated from sulphide analyses (Pearson et al., 2002a; Pearson et al., 2002b). These ancient ages, although few in number, are close to the initiation of the main crust-building events on each craton. Hence, when whole rocks are selected that have undergone minimal metasomatic disturbance, as shown by combined PGE–Os isotope systematics, depletion ages are produced that overlap the sulphide ages. Combined PGE and Re–Os isotope systematics therefore provide a potential means to evaluate the validity of Re–Os isotope model ages.

The complexity of the PGE patterns shown by the Lesotho peridotites analysed here, combined with their strong positive $(Pd/Ir)_n$–$^{187}Os/^{188}Os$ correlation (Fig. 10) and highly variable S contents (Fig. 8), shows that they have experienced significant metasomatic disturbance and sulphide mobility. However, there is a cluster of data on Fig. 10, where the least radiogenic γ_{Os} values are associated with very low $(Pd/Ir)_n$ (<0.1). These samples show PGE patterns very similar in shape and level of Pd/Ir fractionation to the "residual" sulphides identified in peridotites by Alard et al. (2000). Pt/Os ratios are also low in many of these samples, such that their PGE patterns have similar shapes to the "residual" sulphides of Alard et al. (2000). As such, it seems reasonable to assume that the PGE characteristics and hence Os isotope systematics of these samples are strongly influenced by residual, non-metasomatic sulphides.

If the Lesotho peridotites had remained completely closed to disturbance since melting, chondrite-normalised Re abundances should be at least as low as Pd abundances. Only one sample (LQ-8) fits this criteria (Fig. 5). Hence, some Re disturbance has taken place in most of the low $(Pd/Ir)_n$ Lesotho peridotites since melting. The lack of correlation of Re/Os with Os isotopic composition, combined with other petrographic criteria, indicates that this disturbance was recent, most likely associated with kimberlite eruption (Irvine et al., 2001; Simon et al., 2003). The oldest and most common Re depletion ages for the Lesotho peridotites are 2.9–3.0 Gyr (Irvine et al., 2001). These model ages result from samples with the most P-PGE-depleted PGE patterns. As such, they could be interpreted as the true age of melting of these rocks. However, older Re depletion ages for Lesotho bulk rock xenoliths (Pearson et al., 1995) and Re–Os model ages for sulphides from N. Lesotho xenoliths (Griffin et al., 2002) of 3.5 Gyr or greater have been reported. Hence, at least some lithospheric mantle beneath N. Lesotho is of meso-Archean age. Also, it is possible that even though the Lesotho peridotites analysed here have very P-PGE-depleted patterns, their bulk rock Os isotopic compositions are still influenced by enough high Re/Os, high Pt/Os, high γ_{Os} secondary sulphide to alter the minimum Re depletion ages by up to 0.5 Gyr. Alternatively, the older events recorded by the sulfide ages reflect an earlier melting event that did not lead to the formation of lithospheric mantle.

Evidence for significant sulphide mobility in the Lesotho peridotites lies in their highly variable S contents (Fig. 8) that are mostly well above the melt-extraction correlation line defined by massif peridotites (Lorand, 1991). The prominent mode in the whole rock Re depletion ages of 2.9–3.0 Ga (Irvine et al., 2001) is also observed in the sulphide data of Griffin et al. (2002). This may record a second melting event that led to the accretion of the mantle to the lithosphere or an event that introduced new mantle Os to preexisting lithospheric mantle (Pearson et al., 1995; Griffin et al., 2002). If a craton modifying event, this may correlate with the widespread introduction of orthopyroxene into the Kaapvaal cratonic root (e.g., Kelemen et al., 1998). The 2.9–3.0-Gyr model ages of the peridotites could date this orthopyroxene addition.

5.2.2. Namibian peridotite xenoliths

PGE patterns for Namibian peridotites are considerably less fractionated (P-PGE depleted) than the cratonic Lesotho suite (Fig. 5). This observation is in keeping with lower levels of melt depletion, manifest by their major-element systematics (Fig. 1; Table 2). Re-depletion ages show a substantial range from <1 up to 2.2 Gyr. The lowest $(Pd/Ir)_n$ values are considerably higher than those of the most P-PGE-depleted Lesotho samples, but appear appropriate for residues of approximately 30% or more partial melt extraction. Three out of four samples with the lowest $(Pd/Ir)_n$ give Re depletion ages of 2.1–2.2 Ga. This Proterozoic age matches the age of the basement in this area (Hoal et al., 1995; Pearson et al., 2002a) and could be a realistic age for depletion, especially considering the non-cratonic major-element characteristics of these rocks (Boyd et al., 2004). This does not rule out the possibility that the whole rocks are substantially influenced by the high γ_{Os} secondary sulphides. As such, the original melt-depletion age could be older than Paleo-Proterozoic and may even be Archean. However, for this to be the case, the whole suite would have to have experienced total overprinting of major elements and PGE–Os isotope systematics. We note that almost 50 bulk rock Os isotope analyses have now been made on peridotites surrounding the Kaapvaal craton, in areas of Proterozoic crust, and none give any indication of an Archean age (Pearson et al., 2002a).

5.2.3. Vitim peridotite xenoliths

The varied Os isotope compositions of the Vitim peridotites show an excellent correlation with Al_2O_3 (Fig. 7) that could be interpreted as resulting from melt depletion. Based on the similar partition coefficient of Re and Al during melting, Reisberg and Lorand (1995) proposed that extrapolation of such trends to $Al_2O_3 = 0$ gives an initial Os isotope ratio that can be used to calculate the Re depletion model age of the peridotite. Pearson (1999a,b) has suggested that this procedure is not valid because S will be quantitatively removed during melting, and hence, Re/Os will approach zero, whereas Al2O3, even in the most depleted residues, rarely approaches zero. Hence "alumachron" ages are likely to overestimate the melting age of the rock. If the Vitim Al–Os isotope trend is extrapolated to the *y*-intercept, it

yields an initial 187Os/188Os of 0.1086, giving a Re-depletion model age of 2.8 Gyrs. A correlation between CaO and 187Os/188Os also exists, with a shallower trend, producing an initial ratio equivalent to a Re-depletion age of 1.8 Gyr. However, the widely varying Ca/Al of the Vitim suite suggests possible post-melting modification to both these elements, and so, age estimates based on correlations involving these elements are subject to error. It is possible that the Ca–Al–187Os/188Os correlations are a product of metasomatism of a sulphide-saturated silicate melt that introduced silicate phases (diopside and possibly garnet), disturbing Ca/Al. Sulphide precipitation and mobilisation during this event disturbed Pd/Ir, Re/Os and may have also introduced more radiogenic, convecting mantle-derived Os. The combined effects may have created the correlations between Os isotopic compositions and Ca and Al contents.The sample with the lowest $(Pd/Ir)_n$ and least radiogenic Os isotope composition (314-5) gives a minimum Re depletion age (T_{RD}) of 1.8 Gyr. This T_{RD} age, although a minimum, is similar to the Sm–Nd and Rb–Sr clinopyroxene model ages in these rocks (Ionov and Jagoutz, 1989). Although it is tempting to interpret the Nd model ages of the clinopyroxenes as melting ages, because they have Sm/Nd>chondritic, the full REE patterns of this mineral are LREE enriched (Ionov, 2004) and not consistent with a residual character. Nonetheless, a 1.8-Gyr age for lithospheric stabilisation in this region is consistent with available geological evidence. An Archean age for the formation of the lithosphere in the Vitim region seems unlikely based on the major-element composition and mineral chemistry of the peridotites and their striking difference compared to peridotites from the Siberian lithosphere (Boyd et al., 1997).

5.2.4. Beni Bousera massif peridotites

The Beni Bousera peridotites show the narrowest range in Os isotope compositions of the suites analysed. Both Re/Os and Al_2O_3 are correlated with Os isotope composition (Fig. 7) reflecting the depletion in Re as the degree of melting increases (Reisberg and Lorand, 1995). The scatter is indicative of disturbance by alteration or metasomatism. One peridotite, GP 91, has an anomalously high Os and low Re such that its T_{RD} and T_{MA} model ages agree well (1.0 and 1.2 Gyr). Although the high Os content (17 ppb) could be a result of secondary sulphide infiltration, the 1.2-Gyr ($\pm$ 0.2) Re–Os model age is in agreement with the more precise 1.43 ± 0.07 Gyr (2σ) clinopyroxene Lu–Hf isochron age obtained for these peridotites (Pearson and Nowell, 2003). This age also corresponds to estimates of the age of melting in the geologically similar Ronda massif based on Sm–Nd and Re–Os isotope systematics (Reisberg et al., 1991; Reisberg and Lorand, 1995). Hence, an age of 1.2–1.4 Gyr is the likely age of melting and separation of the Beni Bousera peridotites into the lithospheric mantle.

5.2.5. The interpretation of sulphide Re–Os model ages

It is possible to interpret any situation where a peridotite containing sulphide with $^{187}Os/^{188}Os$ lower than the whole rock value as meaning that the sulphide depletion age provides a more realistic estimate of the timing of lithosphere formation than that of the whole rock (e.g., Pearson et al., 2001; Alard et al., 2002; Griffin et al., 2002). However, the possibility of inheritance of older grains, residual from previous melting events that do not relate to lithosphere accretion events, should be considered carefully. The extremely high partition coefficients for Os in sulphide and alloy phases mean that they are unlikely to homogenise their isotopic compositions in the mantle over Gyr timescales. In this way, it is possible for a phase to record a partial melting event that does not relate to the time at which the bulk rock accreted to the lithosphere. For instance, ancient Re–Os model ages, in excess of 1 Gyr, have been recorded in modern samples of oceanic lithosphere that accreted no more than 200 Myr ago (e.g., Brandon et al., 2000). These examples are likely to result from the whole rock being dominated by ''inherited'' sulphide grains that record melting events unrelated to the formation of the oceanic lithosphere in which they now reside. The same principles can be applied to xenoliths. For instance, if sulphide grains with Archean ages were to be found in peridotites which give whole rock Os depletion ages that are Proterozoic, such as the Namibian xenoliths or those of the Beni Bousera massif, it would be unwise to automatically assume that the sulfide ages indicate lithosphere formation in the Archean followed by subsequent reworking. As

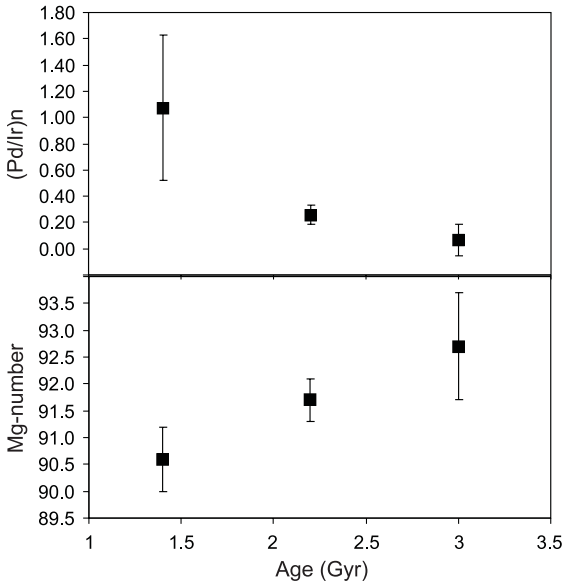

Fig. 12. Maximum Re depletion model age (T_{RD}; based on Os isotope systematics) versus $(Pd/Ir)_n$ and Mg number for Lesotho (cratonic), Namibian (circum-cratonic) and Beni Bousera (orogenic massif) peridotites. Error bars are 1 S.D. of a weighted mean that excludes samples with PGE patterns that show clear disturbances in P-PGE, e.g., with significantly supra-chondritic $(Pd/Ir)_n$ in the case of the xenoliths, or anomalously low Ir values. Vitim average not plotted due to the complex history experienced by this suite.

such, more stringent evaluation of sulfide–whole rock relationships are required to adequately interpret the age information that they provide.

5.3. Secular variation in PGE fractionation and mantle melting

The different ages of the peridotite suites analysed here allow some assessment of the variation of mantle melting PGE fractionation through geological time to form continental lithospheric mantle. The positive correlation shown between Mg number (Fig. 12) or Al_2O_3 content and depletion age for these suites is consistent with a decrease in the degree of mantle melting with time, probably associated with declining mantle temperatures. If weighted means of $(Pd/Ir)_n$ are calculated for the Lesotho, Namibian and Beni Bousera peridotite suite, that filter out anomalous values clearly related to post-melting disturbance, there is a strong inverse correlation with depletion age (Fig. 12). Similarly low $(Pd/Ir)_n$ values are observed in Archean peridotite xenoliths from the Jericho kimberlite, N. Canada (Irvine et al., 2003) and appear a characteristic of Archean melting residues. The highly P-PGE-depleted melt residues produced in the Archean are thus consistent with the notion of elevated mantle temperatures producing larger melt fractions (e.g., Bickle, 1986). The less major-element and P-PGE-depleted melt residues produced later in Earth history are either a result of progressively decreasing mantle temperatures or a change in the mechanism of continental lithosphere generation or both.

Acknowledgements

We thank Geoff Nowell and Chris Ottley for technical assistance. Geoff Nowell is also thanked for timely help with manuscript preparation. We thank Igor Puchtel, Monica Handler and Cin-Ty Lee for constructive reviews and Jean-Pierre Lorand for editorial advice, all of which led to the improvement of this manuscript. This study was supported by a JREI/HEFCE grant DUPEEQ to DGP and a NERC research studentship to GJI. **[RR]**

References

Alard, O., Griffin, W.L., Lorand, J.P., Jackson, S.E., O'Reilly, S.Y., 2000. Non-chondritic distribution of the highly siderophile elements in mantle sulphides. Nature 407, 891–894.

Alard, O., Griffin, W.L., Pearson, N.J., Lorand, J.P., O'Reilly, S.Y., 2002. New insights into the Re–Os systematics of sub-continental lithospheric mantle from in situ analysis of sulphides. Earth Planet. Sci. Lett. 203, 651–663.

Barnes, S.-J., Naldrett, A.J., Gorton, M.P., 1985. The origin of the fractionation of platinum-group elements in terrestrial magmas. Chem. Geol. 53, 303–323.

Bickle, M.J., 1986. Implications of melting for stabilisation of the lithosphere and heat loss in the Archaean. Earth Planet. Sci. Lett. 80, 314–324.

Boyd, F.R., 1989. Compositional distinction between oceanic and cratonic lithosphere. Earth Planet. Sci. Lett. 96, 15–26.

Boyd, F.R., Mertzman, S.A., 1987. Composition and structure of the Kaapvaal lithosphere, Southern Africa. In: Mysen, B.O. (Ed.), Magmatic Processes: Physicochemical Principles. The Geochemical Society, Houston Texas, pp. 3–12.

Boyd, F.R., Pokhilenko, N.P., Pearson, D.G., Mertzman, S.A., Sobolev, N.V., Finger, L.W., 1997. Composition of the Siberian cratonic mantle: evidence from Udachnaya peridotite xenoliths. Contrib. Mineral. Petrol. 128, 228–246.

Boyd, F.R., Pearson, D.G., Hoal, K.O., Hoal, B.G., Nixon, P.H., Kingston, M.J., Mertzman, S.A., 2004. Garnet lherzolites from Louwrencia, Namibia: bulk composition and P/T relations. Lithos, In press.

Brandon, A.D., Walker, R.J., Morgan, J.W., Norman, M.D., Prichard, H.M., 1998. Coupled ^{186}Os and ^{187}Os evidence for core–mantle interaction. Science 280, 1570–1573.

Brandon, A.D., Snow, J.E., Walker, R.J., Morgan, J.W., Mock, T.M., 2000. ^{190}Pt–^{186}Os and ^{187}Re–^{187}Os systematics of abyssal peridotites. Earth Planet. Sci. Lett. 177, 319–335.

Brenan, J.M., Andrews, D., 2001. High-temperature stability of laurite and Ru–Os–Ir alloy and their role in PGE fractionation in mafic magmas. Can. Mineral. 39, 341–360.

Burnham, O.M., Rogers, N.W., Pearson, D.G., van Calsteren, P.W., Hawkesworth, C.J., 1998. The petrogenesis of the Eastern Pyrenean peridotites: an integrated study of their whole-rock geochemistry and Re–Os isotope composition. Geochim. Cosmochim. Acta 62, 2293–2310.

Carlson, R.W., Pearson, D.G., Boyd, F.R., Shirey, S.B., Irvine, G., Menzies, A.H., Gurney, J.J., 1999. Regional age variation of the southern African mantle: significance for models of lithospheric mantle formation. In: Gurney, J.J., Gurney, J.L., Pascoe, M.D., Richardson, S.H. (Eds.), Proc. 7th Int. Kimberlite Conf. Cape Town. National Book Printer, Goodwood, S. Africa, pp. 99–108.

Davis, G.L., Krogh, T.E., Erlank, A.J., 1976. The ages of zircons from kimberlites from South Africa. Carneg. Inst. Wash. Yearbook 75, 821–824.

Dreibus, G.Th., Palme, H., Spettel, B., Zipfel, J., Wanke, H., 1995. Sulfur and selenium in chondritic meteorites. Meteoritics 30, 439–445.

Frey, F.A., Suen, C.J., Stockman, H.W., 1985. The Ronda high temperature peridotite: geochemistry and petrogenesis. Geochim. Cosmochim. Acta 49, 2469–2491.

Griffin, W.L., O'Reilly, S.Y., Pearson, N.J., Graham, S., 2002. In situ Re–Os dating of sulfides in Kaapvaal xenoliths. Geochim. Cosmochim. Acta 66 (S1), A292 (abstract).

Gros, M., Lorand, J.-P., Luguet, A., 2002. Analysis of platinum group elements and gold in geological materials using NiS fire assay and Te coprecipitation; the NiS dissolution step revisited. Chem. Geol. 185, 179–190.

Gueddari, K., Piboule, M., Amosse, J., 1996. Differentiation of platinum group elements (PGE) and of gold during partial melting of peridotites in the lherzolitic massifs of the Betico–Rifean range (Ronda and Beni Bousera). Chem. Geol. 134, 181–197.

Handler, M.R., Bennett, V.C., 1999. Behaviour of platinum-group elements in the subcontinental mantle of eastern Australia during variable metasomatism and melt depletion. Geochim. Cosmochim. Acta 63, 3597–3618.

Handler, M.R., Bennett, V.C., Dreibus, G., 1999. Evidence from correlated Ir/Os and Cu/S for late-stage Os mobility in peridotite xenoliths: implications for Re–Os systematics. Geology 27, 75–78.

Hoal, B.G., Hoal, K.E.O., Boyd, F.R., Pearson, D.G., 1995. Age constraints on crustal and mantle lithosphere beneath the Gibeon kimberlite field, Namibia. S. Afr. J. Geol. 98 (2), 112–118.

Ionov, D., 2004. Chemical variations in peridotite xenoliths from Vitim Siberia: inferences for REE and Hf behaviour in the garnet-facies upper mantle. J. Petrol. 45, 343–367.

Ionov, D.A., Jagoutz, E., 1989. Isotopic behaviour of strontium and neodymium in minerals of garnet- and spinel-containing peridotite xenoliths of the Vitim Plateau: first data from the USSR. Trans. (Doklady) USSR Acad. Sci.: Earth Sci. Sect. 301, 232–236.

Ionov, D.A., Hoefs, J., Wedepohl, K.H., Wiechert, U., 1992. Contents and isotopic composition of sulphur in ultramafic xenoliths from central Asia. Earth Planet. Sci. Lett. 111, 269–286.

Ionov, D.A., Ashchepkov, I.V., Stosch, H.-G., Witt-Eickschen, G., Seck, H.A., 1993. Garnet peridotite xenoliths from the Vitim volcanic field, Baikal region: the nature of the garnet–spinel peridotite transition zone in the continental mantle. J. Petrol. 34, 1141–1175.

Ionov, D.A., Harmon, R.S., France-Lanord, C., Greenwood, P.B., Aschepkov, I.V., 1994. Oxygen isotope composition of garnet and spinel peridotites in the continental mantle: evidence from the Vitim xenolith suite, southern Siberia. Geochim. Cosmochim. Acta 58, 1463–1470.

Irvine, G.J., 2002. Time constraints on the formation of lithospheric mantle beneath cratons: a Re–Os isotope and platinum group element study of peridotite xenoliths from Northern Canada and Lesotho. PhD. Thesis, University of Durham, 384 pp.

Irvine, G.J., Pearson, D.G., Carlson, R.W., 2001. Lithospheric mantle evolution in the Kaapvaal craton: a Re–Os isotope study of peridotite xenoliths from Lesotho kimberlites. Geophys. Res. Lett. 28, 2505–2508.

Irvine, G.J., Pearson, D.G., Carlson, R.W., Kjarsgaard, B.A., Dreibus, G., 2003. Evolution of the lithospheric mantle beneath northern Canada: a Re–Os isotope and platinum group element study of Kimberlite-derived peridotite xenoliths from Somerset Island and a comparison to the Slave and Kaapvaal cratons. Lithos 71, 461–488.

Jagoutz, E., Palme, H., Baddenhausen, H., Blum, K., Cendales, M., Dreibus, G., Spettel, B., Lorenz, V., Wanke, H., 1979. The abundances of major, minor and trace elements in the earth's mantle as derived from primitive ultramafic nodules. Procs. 10th Lunar and Planetary Science Conference, 2031–2050 Pergamon.

Kelemen, P.B., Hart, S.R., Bernstein, S., 1998. Silica enrichment in the continental upper mantle via melt/rock reaction. Earth Planet. Sci. Lett. 164, 387–406.

Kornprobst, J., 1969. Le massif ultrabasique des Beni Bouchera (Rif Interne, Maroc). Contrib. Mineral. Petrol. 29, 283–322.

Lee, C.-T., 2002. Platinum-group element geochemistry of peridotite xenoliths from the Sierra Nevada and the Basin and Range, California. Geochim. Cosmochim. Acta 66, 3987–4005.

Lorand, J.-P., 1991. Sulphide petrology and sulphur geochemistry of orogenic lherzolites: a comparative study of the Pyrenean bodies (France) and the Lanzo Massif (Italy). J. Petrol. Special Lherzolites, 77–95.

Lorand, J.-P., Alard, O., 2001. Platinum-group element abundances in the upper mantle: new constraints from in situ and whole-rock analyses of Massif Central xenoliths. Geochim. Cosmochim. Acta 65, 2789–2806.

Lorand, J.-P., Keays, R.R., Bodinier, J.L., 1993. Copper and noble

metal across the lithosphere–asthenosphere boundary of mantle diapirs: evidence from the Lanzo lherzolite massif. J. Petrol. 34, 1111–1140.

Lorand, J.-P., Pattou, L., Gros, M., 1999. Fractionation of Platinum-group elements and gold in the upper mantle: a detailed study in Pyrenean orogenic lherzolites. J. Petrol. 40, 957–981.

Lorand, J.-P., Schmidt, G., Palme, H., Kratz, K.-L., 2000. Highly siderophile element geochemistry of the earth's mantle: new data for the Lanzo (Italy) and Ronda (Spain) orogenic peridotite bodies. Lithos 53, 149–164.

Lorand, J.-P., Reisberg, L., Bedini, R.M., 2003. Platinum-group elements and melt percolation processes in Sidamo spinel peridotite xenoliths, Ethiopia, East African Rift. Chem. Geol. 196, 57–75.

Luguet, A., Alard, O., Lorand, J.P., Pearson, N.J., Ryan, C.G., O'Reilly, S.Y., 2001. Laser-ablation microprobe (LAM)-ICP-MS unravels the highly siderophile element geochemistry of the oceanic mantle. Earth Planet. Sci. Lett. 189, 285–294.

Luguet, A., Lorand, J.-P., Seyler, M., 2003. Sulfide petrology and highly siderophile element geochemistry of abyssal peridotites: a coupled study of samples from the Kane Fracture Zone (45°W 23°20N, MARK Area, Atlantic Ocean). Geochim. Cosmochim. Acta 67, 1553–1570.

McDonough, W.F., Suns, S.S., 1995. The composition of the earth. Chem. Geol. 120, 223–253.

Meisel, T., Moser, J., Fellner, N., Wegscheider, W., Schoenberg, R., 2001a. Simplified method for the determination of Ru, Pd, Re, Os, Ir and Pt in chromitites and other geological materials by isotope dilution ICP-MS and acid digestion. Analyst 126, 322–328.

Meisel, T., Walker, R.J., Irving, A.J., Lorand, J.-P., 2001b. Osmium isotopic compositions of mantle xenoliths: a global perspective. Geochim. Cosmochim. Acta 65, 1311–1323.

Mitchell, R.H., Keays, R.R., 1981. Abundance and distribution of gold, palladium and iridium in some spinel and garnet lherzolites: implications for the nature and origin of precious metal-rich intergranular components in the upper mantle. Geochim. Cosmochim. Acta 45, 2425–2442.

Morgan, J.W., 1986. Ultramafic xenoliths: clues to Earth's late accretionary history. J. Geophys. Res. 91 (B12), 12375–12387.

Morgan, J.W., Wandless, G.A., Petrie, R.K., Irving, A.J., 1981. Composition of the Earth's upper mantle: I. Siderophile trace elements in ultramafic nodules. Tectonophysics 75, 47–67.

Morgan, J.P., Walker, R.J., Brandon, A.D., Horan, M.F., 2001. Siderophile elements in the Earth's upper mantle and lunar breccias: data synthesis suggests manifestations of the same late influx. Meteorol. Planet. Sci. 36, 1257–1275.

Pattou, L., Lorand, J.P., Gros, M., 1996. Non-chondritic platinum-group element ratios in the Earth's mantle. Nature 379, 712–715.

Pearson, D.G., 1989. The petrogenesis of pyroxenites containing octahedral graphite and associated mafic and ultramafic rocks of the Beni Bousera peridotite massif. N. Morocco. PhD Thesis, Leeds, 413 pp.

Pearson, D.G., 1999a. The age of continental roots. Lithos 48, 171–194.

Pearson, D.G., 1999b. Evolution of cratonic lithospheric mantle: an isotopic perspective. In: Fei, Y., Bertka, C.M., Mysen, B.O. (Eds.), Mantle petrology: field observations and high pressure experimentationSpec. Pub. Geochem. Soc., vol. 6, pp. 57–78. Houston.

Pearson, D.G., Nowell, G.M., 2003. Dating mantle differentiation: a comparison of the Lu–Hf, Re–Os and Sm–Nd isotope systems in the Beni Bousera peridotite massif and constraints on the Nd–Hf composition of the lithospheric mantle. Geophys. Res. Absts. 5, 05430.

Pearson, D.G., Nowell, G.M., 2004. Re–Os and Lu–Hf isotope constraints on the origin and age of pyroxenites from the Beni Bousera peridotite massif: implications for mixed peridotite–pyroxenite melting models. J. Petrol 45, 439–455.

Pearson, D.G., Woodland, S.J., 2000. Carius tube digestion and solvent extraction/ion exchange separation for the analysis of PGEs (Os, Ir, Pt, Pd, Ru) and Re–Os isotopes in geological samples by isotope dilution ICP–mass spectrometry. Chem. Geol. 165, 87–107.

Pearson, D.G., Davies, G.R., Nixon, P.H., 1993. Geochemical constraints on the petrogenesis of diamond facies pyroxenites from the Beni Bousera peridotite massif, north Morocco. J. Petrol. 34, 125–172.

Pearson, D.G., Carlson, R.W., Shirey, S.B., Boyd, F.R., Nixon, P.H., 1995. The stabilisation of Archaean lithospheric mantle: a Re–Os isotope study of peridotite xenoliths from the Kaapvaal craton. Earth Planet. Sci. Lett. 134, 341–357.

Pearson, D.G., Shirey, S.B., Harris, J.W., Carlson, R.W., 1998. A Re–Os isotope study of sulfide diamond inclusions from the Koffiefontien kimberlite, S. Africa: Constraints on diamond crystallisation ages and mantle Re–Os systematics. Earth Planet. Sci. Lett. 160, 311–326.

Pearson, D.G., Irvine, G.J., Carlson, R.W., Kopylova, M.G., Ionov, D.A., 2002a. The development of lithospheric mantle keels beneath the earliest continents: time constraints using PGE and Re–Os isotope systematics. In: Fowler, C.M.R., Ebinger, C.J., Hawkesworth, C.J. (Eds.), The Early Earth: Physical, Chemical and Biological Development. Geol. Soc. (Lond.) Spec. Pub., vol. 199, 65–90. London.

Pearson, N.J., Alard, O., Griffin, W.L., Jackson, S.E., O'Reilly, S., 2002b. In situ measurement of Re–Os isotopes in mantle sulfides by laser ablation multicollector inductively coupled plasma mass spectrometry: analytical methods and preliminary results. Geochim. Cosmochim. Acta. 66, 1037–1050.

Pearson, D.G., Canil, D., Shirey, S.B., 2003. Mantle samples included in volcanic rocks: xenoliths and diamonds. In: Holland, H.D., Turekian, K.K. (Eds.), Treatise on Geochemistry, vol. 2. Elsevier, Amsterdam, pp. 171–275. Chapter 5, In press.

Puchtel, I.S., Humayun, M., 2000. Platinum group elements in Kostomuksha komatiites and basalts: implications for oceanic crustal recycling and core–mantle interaction. Geochim. Cosmochim. Acta 64, 4227–4242.

Puchtel, I.S., Humayun, M., 2001. PGE fractionation in a komatiitic basalt lava lake. Geochim. Cosmochim. Acta 67, 2979–2993.

Rehkämper, M., Halliday, A.N., Barford, D., Fitton, J.G., Dawson, J.B., 1997. Platinum-group element abundance patterns in different mantle environments. Science 278, 1595–1598.

Rehkämper, M., Halliday, A.N., Alt, J., Fitton, J.G., Zipfel, J.,

Wood, S.A., 1999a. Non-chondritic platinum-group element ratios in oceanic mantle lithosphere: petrogenetic signature or melt percolation? Earth Planet. Sci. Lett. 172, 65–81.

Rehkämper, M., Halliday, A.N., Fitton, J.G., Lee, D.-C., Wieneke, M., Arndt, N.T., 1999b. Ir, Ru, Pt and Pd in basalts and komatiites: new constraints for the geochemical behaviour of the platinum-group elements in the mantle. Geochim. Cosmochim. Acta 63, 3915–3934.

Reisberg, L., Lorand, J.P., 1995. Longevity of sub-continental mantle lithosphere from osmium isotope systematics in orogenic peridotite massifs. Nature 376, 159–162.

Reisberg, L.C., Allegre, C.J., Luck, J.-M., 1991. The Re–Os systematics of the Ronda ultramafic complex in southern Spain. Earth Planet. Sci. Lett. 105, 196–213.

Righter, K., Downs, R.T., 2001. The crystal structure of synthetic Re- and PGE-bearing magnesioferrite spinels: implications for impacts, accretion and the mantle. Geophys. Res. Lett. 28, 619–622.

Roy-Barman, M., Luck, J.M., Allegre, C.J., 1996. Os isotopes in orogenic lherzolite massifs and mantle heterogeneities. Chem. Geol. 130, 55–64.

Saal, A.E., Takazawa, E., Frey, F.A., Shimizu, N., Hart, S.R., 2001. Re–Os isotope in the Horoman peridotite: evidence for refertilisation? J. Petrol. 42, 25–37.

Simon, N.S.C., Irvine, G.J., Davies, G.R., Pearson, D.G., Carlson, R.W., 2003. The origin of garnet and clinopyroxene in depleted Kaapvaal peridotites. Lithos 71, 289–322.

Snow, J.E., Schmidt, G., 1998. Constraints on Earth accretion deduced from noble metals in the oceanic mantle. Nature 391, 166–169.

Walter, M.J., 1999. Melting residue of fertile peridotite and the origin of cratonic lithosphere. In: Fei, Y., Bertka, C.M., Mysen, B.O. (Eds.), Mantle Petrology: Field Observations and High Pressure ExperimentationSpec. Pub. Geochem. Soc. vol. 6, 225–239 Houston.

Walter, M.J., 2003. Melt extraction and compositional variability in the mantle. In: Holland, H.D., Turekian, K.K. (Eds.), Treatise on Geochemistry, vol. 2. Elsevier, Amsterdam, pp. 363–394. Chapter 8.

Wood, S.A., 1987. Thermodynamic calculations of the volatility of the platinum group elements (PGE): the PGE content of fluids at magmatic temperatures. Geochim. Cosmochim. Acta 51, 3041–3050.